

---

# The Circulatory System: from Case Studies to Mathematical Modeling

Luca Formaggia<sup>1</sup>, Alfio Quarteroni<sup>1,2</sup>, and Alessandro Veneziani<sup>1</sup>

<sup>1</sup> MOX, Department of Mathematics, Politecnico di Milano, Piazza L. da Vinci 32, Milano, Italy

<luca.formaggia,alfio.quarteroni,alessandro.veneziani>@mate.polimi.it

<sup>2</sup> CMCS-IACS, Ecole Polytechnique Federale de Lausanne, Station 8, Lausanne, Switzerland [alfio.quarteroni@epfl.ch](mailto:alfio.quarteroni@epfl.ch)

**Summary.** In this work we illustrate some real case studies in vascular medicine and surgery that we have recently investigated with the support of mathematical models and numerical simulations. More precisely, we present six examples, where our investigation has different purposes, ranging from a better understanding of phenomena of clinical interest to the optimization of surgical procedures. For each case, the description of the problem is followed by the illustration of the mathematical model and the numerical technique used for its investigation, including the discussion of some numerical results. Each example thus provides the conceptual framework to introduce mathematical models and numerical methods whose applicability, however, goes beyond the specific case that is addressed.

**Key words:** Blood Flow Modeling, Computational Haemodynamics, Vascular Diseases and Surgical Planning

## 1 An Overview of Vascular Dynamics and Its Mathematical Features

The use of mathematical models, originally radicated mainly in sectors with a strong technical content (such as, e.g., automotive and aerospace engineering), is now widespread also in many fields of life sciences, where often human factors prevail. Bioinformatics, mathematical analysis and scientific computing support investigations in different fields of biology (like genetics or physiology) and medicine. Mathematical models and numerical simulations can for example establish a bond between molecular structures and clinically evident behavioral patterns. Providing quantitative data on the behavior of organs, systems, or even the entire body, in terms of subcellular functions, they can as well contribute through the interpretation of medical images, and maps of

electric potentials, to the definition of therapies and to the design of medical devices.

One subject that has caught the attention of important mathematicians and scientists in the past (from Aristoteles to Bernoulli, Euler, Poiseuille and Young) is the functioning of the cardiocirculatory system. Recently, the socio-economic impact of cardiovascular pathologies has further motivated this research, which presents challenging mathematical difficulties. Up to the Seventies, *in vitro* and animal experiments were the main means of investigation in this field. Yet, the progress in computational fluid dynamics as well as the increase in computer power has added the numerical experiments to the tools at disposal to medical researchers, biologists and bioengineers. Quantities like shear stresses on the endothelium surface, which are quite hard, if not impossible, to measure *in vitro*, can now be calculated from simulations carried out on real geometries obtained with three-dimensional reconstruction algorithms. In this respect, a decisive thrust has been provided by the development of modern non-invasive data collection technologies, like nuclear magnetic resonance, digital angiography, CT scans and Doppler anemometry (see e.g. [Ste02]).

The separation of the blood flow and the generation of a secondary motion are today recognized as potential factors for the development of arterial pathologies (such as atherosclerotic plaques formation). They may be induced by a particular vascular morphology, like a bifurcation; an example related to the carotid artery is illustrated in the left picture of Fig. 1. A detailed understanding of the local haemodynamic patterns and of their effects on the vessel wall is today a possibility thanks to accurate computer simulations.

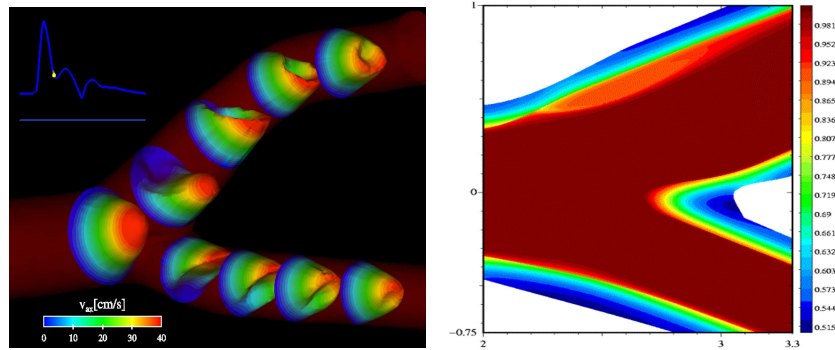


**Fig. 1.** On the left: velocity profiles computed in a carotid bifurcation at the end of the systole (courtesy of M. Prosi). On the right: simulations of the concentration of oxygen in the lumen and the wall of a carotid bifurcation (courtesy of P. Zunino)

In large arteries, blood flow interacts mechanically with the vessel wall, giving rise to a complex fluid-structure interaction mechanism with a conti-

nous transfer of energy between the blood and the vessel structure. Moreover, a thorough investigation of the role of haemodynamics in vascular pathologies needs to monitor the concentration of some relevant chemical components (like oxygen, lipids or, possibly, drugs). The blood flow problem must therefore be coupled with models describing the transport, diffusion and absorption of chemicals in all the various layers that form the arterial wall (intima, media and adventitia). The complexity (and non-linearity) of the coupling is increased by the fact that wall shear stresses influence the orientation and deformation (or even damaging) of the endothelial cells. Consequently, wall permeability typically depends on wall shear stress. Numerical simulations of this type, like the one on the right picture of Fig. 1, can explain the biochemical modifications produced by blood flow alterations caused, for example, by the presence of a stenosis.

*Basic mathematical features of the problem.* We can point out some basic features of the phenomena previously illustrated that drive the choice of the mathematical models and the numerical methods used for their approximation. The first, and perhaps more relevant, is *unsteadiness*. Quoting [NO90], “The most obvious thing of blood flow in arteries is that it is pulsatile”. The arterial pulsatility induced by the the heart action strongly influences hemodynamics. The basic time scale in this context is given by the heart beat (about 0.8 s). We may recognise an initial phase called *systole* (about 0.3 s), when the aortic valve is open and the blood is thrust into the arterial system, followed by the *diastole* (about 0.5 s), initiated by the closure of the aortic valve. Fast transients are therefore a relevant feature of blood flow and specific numerical techniques for their reliable simulations are required, particularly when one is interested in blood flow in large arteries (those whose diameter is above 0.4mm).

*Heterogeneity* is another key feature. In fact, haemodynamics entails different phenomena interacting at different levels. At the mathematical level, this implies the coupling of different models acting either in the same computational domain or in adjacent subdomains and related by appropriate interface or matching conditions. Their numerical treatment may require ad-hoc methods developed on split regions (*domain decomposition techniques*, see [QV99]).

A further important feature of haemodynamics problems is the presence of *multiple scales* in both time and space. An illustrative instance is represented by the (either active or passive) regulation of blood flow distribution. A stenosis in a carotid or a cerebral artery, even when yielding a significant lumen reduction, does not necessarily cause a relevant reduction of blood supply to the downstream compartments. In fact, blood flow is redistributed through secondary vessels and continue to ensure an almost physiological blood flow. These morphological changes are activated by biochemical mechanisms which govern vessel dilatation and may even drive the oxygen exchange between blood and tissues. Here, we face different time scales (blood flow and regulation mechanisms) and spatial scales (the local haemodynamics and the global

circulation). Similar mechanisms are present, for instance, in the Willis circle, making the vascular network in the brain a robust system.

Another example is the onrise and growth of cerebral aneurysms, a major pathology with many aspects still to be clarified. Here, complex interactions involving systemic factors, like hypertension or high cholesterol levels, and local blood flow features associated to particular vascular morphologies can induce the onrise of the pathology. Again, different time scales are involved.

This multiscale nature requires to devise suitable numerical techniques for coupling the different models, capable of reproducing the interaction between small scales phenomena as well as the macroscopic level. In this respect, the term *geometrical multiscale* has been coniated for techniques that account of different space scales involving local and systemic dynamics. Several examples and applications may be found in [FNQV99], [QV03], [FV03a] and [FV05].

*The tasks of computational haemodynamics.* All the features previously listed must be adequately accounted for when developing mathematical models and numerical methods for the circulatory system. The rigorous mathematical derivation of these models is however beyond the scope of these notes; the interested reader can refer, for instance, to [FQ04]. Here, we wish to take a different route. We will present a set of problems arising from realistic clinical cases, and illustrate their specific characteristics that drive the choice of mathematical and numerical models.

The selection of our case studies has been driven by the different objective that one wants to achieve with numerical simulations. A first goal of computational haemodynamics is to help the *understanding of the on-rise and the development of (individual) physiopathologies*.

In general, in the medical field, carrying out in vivo and in vitro experiments has clear practical and ethical limitations, in particular for a deep understanding of the features of the single patient that could be responsible of a pathological behavior. Nowadays, for instance, geometrical reconstructions of an individual carotid morphology starting from angiographies, CT scans or MR images can be extensively used for evaluating the impact of the vessel shape on the wall shear stress and consequently on the possible development of atherosclerotic plaques. Other examples are considered in the present overview. In particular, numerical simulations of the different pulmonary artery banding in neonates affected by left ventriculum hypoplasia, which has clarified the impact of the banded vessel profile on the shear stress and provided a quantitative explanation of the observed follow up on the patients (see Sect. 2.1). Another example addressed here refers to the modifications of the blood flow and metabolic dynamics induced by exercise (like for sport activity), or by the ageing (Sect. 2.2).

Another issue is *prediction and design*. In some engineering fields numerical simulations represent a consolidated tool for supporting design and the set up of a new prototype, with the aim of reducing the more expensive experimental assessment. Quoting [Met03], “Since the late 1950s, CFD (Computational Fluid Dynamics) has played a major role in the development of more

versatile and efficient aircraft. It has now become a crucial enabling technology for the design and development of flight vehicles. No serious aeronautical engineer today would consider advancing a new aircraft design without extensive computational testing and optimization. The potential of CFD to play a similar role in cardio-vascular intervention is very high". With a similar perspective, in this work we will address the design of drug eluting stents. The role of numerical simulations in setting up a coating film ensuring a correct drug delivery is essential (Sect. 2.3). Another example is given by numerical simulations for comparing different possibilities of a surgical intervention in pediatric heart diseases, providing practical indications for the surgeon (Sect. 2.4).

Finally, a third - and perhaps the most ambitious - kind of task is *identification and optimization*. Scientific computing is nowadays used to solve not only direct, but also inverse problems, i.e. to help devising a solution which fulfills some prescribed optimality criteria. The task could be therefore not only to simulate the fluid dynamics in a given vascular district or, more in general, in a *compartment* (i.e. a set of organs and tissues). Rather, the desired dynamics inside the compartment are specified (or given by measures in identification problems), and the computations have the role to identify the "parameters" of the problem ensuring that these features will be fulfilled at best (e.g. the "optimal" shape of a prosthetic implant). The major difficulty in solving optimization problems in general (and for life sciences in particular) is represented by the severe computational costs. Optimization solvers are usually based on iterative procedures and this could be prohibitively expensive if each iteration requires the solution of a system of non-linear time-dependent partial differential equations. For this reason, specific techniques are under development, aiming at reducing the computational costs. Here, we will address two cases. In the first one, optimization has been applied to the set up of a procedure for the so called *peritoneal dialysis* (Sect. 2.5). The optimal solution computed by numerical means has been implemented in an electronic device with the aim of regulating the process specially for each patient. In the second case that we will present, shape optimization techniques, together with specific methods for the reduction of computational costs, are applied to coronary by-pass anastomosis in order to find the "best" post-surgery configuration, which reduces the risk of operation failure (Sect. 2.6).

In Section 3, we will give a synthesis of the different examples considered, highlighting some open problems and perspectives of this interesting and rapidly growing research field.

## 2 Case Studies

We present here a set of examples in the field of computational haemodynamics emerging from real clinical cases we have studied in cooperation with medical doctors, surgeons and bioengineers. Each problem will be first de-

scribed in medical terms, then we will introduce its mathematical formulation and the numerical tools that have been used for its solution.

## 2.1 Numerical investigation of arterial pulmonary bandings

### *The problem*

An artificial regulation of the pulmonary blood flow is sometimes necessary to face some serious heart congenital defects, see [CSB<sup>+</sup>03]. A surgical procedure to achieve this goal consists of banding the pulmonary artery, so that the vessel lumen is suitably modified and the blood flow rate adjusted to the need. As a matter of fact, this technique modifies the pulmonary artery *resistance*<sup>3</sup>. This represents a palliative for pathologies like functional univentricular hearts, multiple ventricular and atrio-ventricula septal defects and, more recently, it has been used in hypoplastic left heart malformations, either as a rescue procedure for critical neonates or as preparatory measure in view of subsequent surgical operations (like the Norwood procedure - see Sect. 2.4 or heart transplant).

The conventional pulmonary artery banding in neonates and infants has however some drawbacks that have limited its use so far. In particular:

1. the banding has to be adapted in time since the blood flow demand is changing with growth;
2. the pulmonary arterial wall is damaged by the procedure to such an extent that frequently a surgical repair procedure is needed after de-banding.

Recently, a new device for arterial banding, called *FloWatch*©-PAB (designed by EndoArt, Lausanne, Switzerland), has been set up, originally to overcome the first limitation. It has later been found that it helps to overcome the second problem too, as we will show next.

The FloWatch system comprises an implantable device and an external control unit. The former features a clip which is placed around the pulmonary artery in a fashion similar to a watch band. The area of the vessel lumen can be adjusted by means of a piston which acts on the clip and is driven by a micro-engine. The engine is electrically activated and controlled by telemetry by means of the external unit. This system, denoted *adjustable pulmonary artery banding*, allows to adapt the banding in time without any further surgical intervention on the patient.

Clinical data have shown that with the FloWatch banding also the second drawback seems to be by-passed. Quoting [CSB<sup>+</sup>03]: “...we didn’t see any lesion in the pulmonary artery in the experimental study... the histology showed in all the cases almost normal pulmonary artery with very pliable tissue.”.

A quantitative analysis of the functioning of the device was carried out by means of numerical simulations as reported in [CPF<sup>+</sup>05] and it has highlighted

---

<sup>3</sup> The *vascular resistance* is related to the vessel lumen and the flow viscosity. It will be introduced in Sect. 2.2.

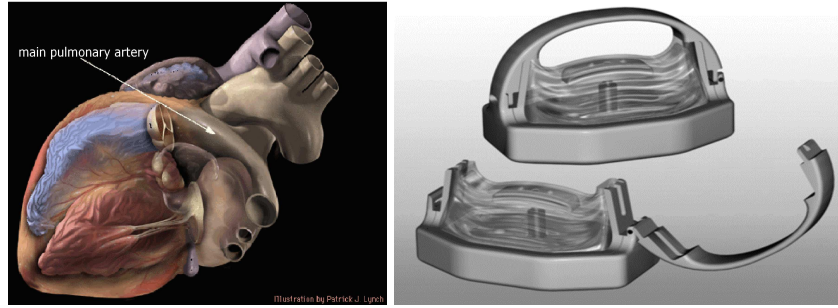


**Fig. 2.** On the left: The heart with the indication of the pulmonary artery where the banding is applied. (Illustration by P. J. Lynch, see [patricklynch.net](http://patricklynch.net)). On the right: FloWatch device in open and closed positions. Notice the banana-shape of the clipping (photo from [CFvSS02])

the relations between the perimeter and the area of the banding, the banding pressure gradients distribution and the induced stresses, comparing them with the traditional approach. The research has been carried out in cooperation with Dr. A. Corno of the Aldler Hey Royal Children Hospital in Liverpool (England).

#### *Numerical models and simulations*

We introduce here some mathematical models that have proved to be well suited for the simulations of the pulmonary arterial banding and we discuss briefly the numerical results.

*Models and Methods.* Let us indicate with  $\mathbf{u}(\mathbf{x}, t)$  and the  $P(\mathbf{x}, t)$  the blood velocity and pressure respectively in the domain  $\Omega_l$ , the vascular lumen. With  $\Omega_w$  we denote the vessel wall (see Fig. 3). The two domains are separated by the so called *endothelial membrane*  $\Gamma_{int}$  and are delimited by the boundaries  $\Gamma_{up}$  (upstream or proximal sections) and  $\Gamma_{dw}$  (downstream or distal sections). Finally, the external boundary of the vascular wall is denoted by  $\Gamma_{ext}$ .

The application of the physical principles of momentum and mass conservation for an incompressible fluid leads to the equations:

$$\begin{cases} \frac{\partial \mathbf{u}}{\partial t} + (\mathbf{u} \cdot \nabla) \mathbf{u} - \nabla \cdot \mathbf{S} + \nabla p = \mathbf{f} \\ \nabla \cdot \mathbf{u} = 0 \\ \mathbf{u}|_{t=0} = \mathbf{u}_0 \end{cases} \quad \mathbf{x} \in \Omega, t \in (0, T] \quad (1)$$

For the sake of simplicity the momentum equation has been divided by the density  $\rho$ , therefore here  $p = P/\rho$  and  $\mathbf{f}$  is a generic field of forces per unit of mass.

The quantity  $\mathbf{S}$  is the so-called *deviatoric* stress tensor and is a function of the velocity. The actual dependence of  $\mathbf{S}$  on  $\mathbf{u}$  is matter of *blood rheology*,

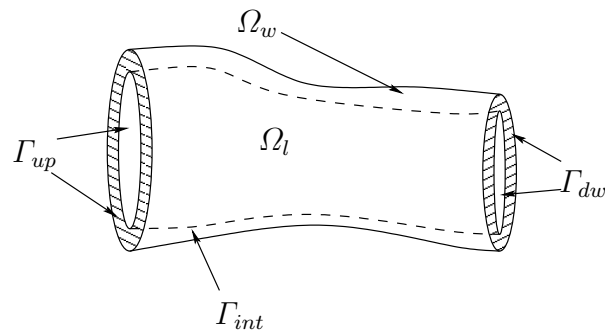


**Fig. 3.** A possible domain in a haemodynamic simulation

i.e. the mathematical description in terms of constitutive laws of the complex interaction between the suspended particles and the behavior of the fluid as a continuum. The adoption of a specific rheological law depends on the features of the particles (in particular the red cells), and on the characteristics of the vascular district at hand. For the derivation of equations (1) and the rheological laws, see e.g. [FQ04] and the bibliography quoted therein. In the case of the pulmonary artery, which has a diameter of about 2 cm, a Newtonian rheology is accurate enough to describe the blood behavior. Here, the deviatoric tensor is proportional to the symmetric part of velocity gradient, namely

$$\mathbf{S} \equiv 2\nu \frac{1}{2} (\nabla \mathbf{u} + \nabla^T \mathbf{u}), \quad (2)$$

where  $\nu$  is the (constant) *kinematic viscosity* of blood.

Equations (1) must be completed with boundary conditions on  $\partial\Omega_l$ . In particular, those on  $\Gamma_{up} \cup \Gamma_{down}$  should account for the presence of the remaining part of the circulatory system. For the purpose of the present study, in which we want to compare the flow conditions induced by different types of banding, it is sufficient to assume that, for  $t > 0$ ,

$$\mathbf{u} = \mathbf{g} \quad \mathbf{x} \in \Gamma_{up}, \quad \text{and} \quad p\mathbf{n} - \mathbf{S} \cdot \mathbf{n} = \mathbf{0}, \quad \mathbf{x} \in \Gamma_{down}. \quad (3)$$

In particular,  $\mathbf{g}$  has been chosen as a Poiseuille parabolic fully developed profile [FQ04].

On  $\Gamma_{int}$  we need to prescribe conditions associated to the interaction between the blood and the vascular wall. In general, the set-up of these conditions is a challenging problem at both the mathematical and numerical level, because of the compliance of the vascular wall. However, for the sake of simplicity, in the present case we have assumed that the wall is rigid, which corresponds to take

$$\mathbf{u} = \mathbf{0}, \quad \mathbf{x} \in \Gamma_{int}, \quad t > 0. \quad (4)$$

Equations (1), (2) are the so called *Navier-Stokes equations* for an incompressible Newtonian fluid. They have been extensively investigated from the

mathematical viewpoint, e.g., in [Tem86]. Together with (3) and (4), they provide the mathematical model for our banding problem.

The description of the computational domain  $\Omega_l$  has been obtained in our case by a geometrical reconstruction from some images taken with a camera, done by using some tools provided by the software *Mathematica* [Wol]. Camera data cover the arterial segment from the pulmonary valve to the section upstream the pulmonary bifurcation. However, since the bifurcation strongly affects the local haemodynamics, we have included it by extending the reconstructed domain with a T-bifurcation (see Fig. 4 left). The diameter of the vascular lumen is here  $D = 18mm$ .

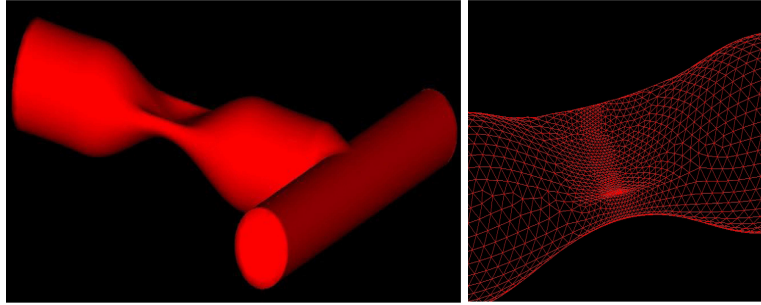


**Fig. 4.** On the left: Computational domain including the pulmonary banding and the pulmonary bifurcation. On the right: Detail of the mesh around the banding (Courtesy of M. Prosi)

For the numerical solution of (1) we have used finite differences for the time derivative and finite elements for the space derivatives [FQ04]. In Fig. 4 (right) we show a detail of the finite element grid around the FloWatch device.

*Results.* Several numerical simulations have been carried out for both the traditional banding and the one produced by the FloWatch. Three levels of occlusion of the lumen have been considered, namely 26%, 50% and 62%, as well as two different flow rates, 1.5 and 2.0 lit/min. The latter have been set by appropriately choosing the Poiseuille inflow datum  $\mathbf{g}$ .

The banding controls the flow by adjusting the vascular resistance. Indeed, a vaso-constriction induces a higher pressure gradient for a given flow rate and, conversely, a reduced flow for a given pressure difference at the ends of the vessel. In a perfect cylindrical domain the ratio between pressure gradient and flow rate is inversely proportional to the section area (see [Whi86]). The first goal of numerical simulations was therefore to investigate the behavior of this quantity in the case of the more complex shape produced by the FloWatch banding (see the picture on the right of Fig. 4).

In Fig. 5 (right) we report the pressure differences obtained with the two bandings for an occlusion of 50% and 26% of the section area, respectively,

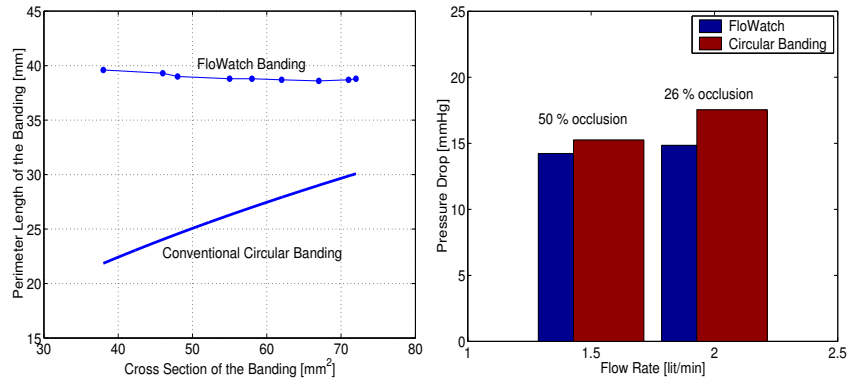


**Fig. 5.** On the left: Section area vs. Section perimeter for the circular and the FloWatch banding, respectively. On the right: Computed pressure difference vs. flow rate for the two type of bandings and different occlusion levels.

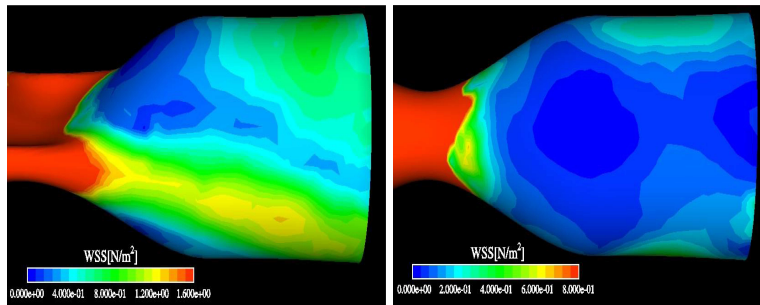


**Fig. 6.** Wall shear stress fields in the FloWatch (left) and circular (right) bandings (Courtesy of M. Prosi)

and for two different input flow rates. The conclusion is that the efficiency is almost independent of the type of banding and is strongly related to the section area. In fact, although the shape induced by the two bandings is very different, the pressure drop for a given flow and occlusion level is rather the same. This is also confirmed by the clinical data reported in [CPF<sup>+</sup>05]. In Fig. 6 we illustrate the computed wall shear stress maps induced by blood in the two cases. It is possible to observe that the conventional circular banding is associated to a lower shear stress field and this is frequently recognized as a possible pathogenic factor in wall tissue degeneration or even atherosclerosis (see e.g. [NL87]).

Another task of the numerical simulations was to investigate the situation after de-banding. It has been observed that with the FloWatch banding the perimeter of the constricted section is lined to the banana-shape section of the FloWatch banding shown in the right picture in Fig. 2. Consequently, it is practically independent of the luminal section area, as shown in the left

picture of Fig. 5, where we have plotted the cross sectional area versus the external perimeter for both the conventional and the FloWatch banding, for the normal range of the constriction level.

A realistic hypothesis is then that, after the removal of the constriction, the pulmonary artery reopens to a circular section having the same perimeter of the banded configuration. Therefore, after the conventional banding the vessel is unable to reopen fully, and this is verified by clinical evidence. Furthermore, it is reasonable to assume that the perimeter reduction induced by the conventional banding yields local stresses in the vessel structure which responds with unwanted morphological changes. Indeed, after removing the conventional band, arterial wall is often found severely damaged, with an increased thickness, dense fibrosis and consequent loss of elasticity and pliability, so that surgical resection and reconstruction is necessary. The reconstruction procedure is an additional intrusive operation and often induces residual undesired resistances in the pulmonary artery.

Using the FloWatch device it has been found that after de-banding the perimeter of the luminal section is only slightly reduced and therefore the residual constriction is not significant. For a 50% occlusion, corresponding to  $39\text{mm}^2$  cross section area, the perimeter after de-banding is of about  $39.5\text{mm}$  which corresponds to a diameter of  $12.6\text{mm}$ , not far from the physiological diameter ( $18\text{mm}$ ). Numerical simulations on the de-banded configuration confirm that the residual pressure drop is in the range of  $2.5\text{mmHg}$  for a flow rate of  $1.5\text{L}/\text{min}$ , which is reasonably small.

Geometrical and numerical analysis have provided a possible interpretation for the clinical evidence, showing that the new FloWatch banding:

1. is effective at all realistic constriction levels, showing the same flow control characteristics of conventional banding;
2. achieves a given area reduction with a smaller contraction of the vessel perimeter. This implies a reduced stress on the banded arterial wall and a better behavior after de-banding, to such an extent that a surgical reconstruction of the pulmonary artery is in general no longer needed.

## 2.2 Numerical investigation of systemic dynamics

### *The problem*

Which are the effects of aging on the vascular system? How does heavy exercise influence the transport by the blood stream of oxygen or other metabolites and their consumption by tissues? Which kind of self-regulatory processes governs the dynamics of blood solutes? Why the implant of an endovascular prosthesis can induce an overload on the heart?

To answer all these questions requires a quite different viewpoint than the one adopted in the previous example. There, the goal was to investigate a *local* process. Here, the answer needs a systemic perspective, able to correlate

actions and reactions in different cardiovascular compartments. The “Digital Astronaut” programme launched in October 2004 by the National Space Biomedical Research Institute of the NASA can be regarded as an ambitious example in this perspective. The long-term task of this program is to develop a model accounting for the mutual interaction of the different parts of the body and able to evaluate the response of the cardiovascular system to different external conditions (see [Rak04]). The final aim is to find countermeasures to the syndromes and pathologies affecting an astronaut living in a low gravity environment for a long period, and to speed-up the return to normal conditions at the end of a mission.

Using appropriate mathematical models we can simulate the regulating processes the human body activates to contrast changes in outside conditions. For instance, the elasticity a blood vessel changes in the absence of gravity as the smooth muscles that surrounds it are controlled by the nervous system, which in turn reacts to biochemical or mechanical variations. Indeed, adjustment and regulation processes are characteristics common to all biological systems: thousands of feedback mechanisms influence the conditions of cells and organs, and are eventually the foundation of life. Such processes are encoded by complex enzymic reactions and are particularly hard to describe in a purely phenomenological and experimental manner, especially in complex organisms like a human being.

The mathematical tools for this simulations cannot be, in general, the same used in the previous Section. Even if we just focus on blood flow dynamics, carrying out a simulation of a large part of the circulatory system by solving the three-dimensional Navier-Stokes equations (1) would require the availability of a large set of morphological data (quite difficult to obtain). Not to mention the high computational costs. Furthermore, in certain vascular compartment the hypothesis of Newtonian rheology would be questionable.

However, the level of detail given by a 3D model is unnecessary when one is primarily interested in the global response. We need therefore to find a reasonable hierarchy of models, with different level of detail, and however sufficiently reliable to answer our questions. Moving from reasonable simplifying assumptions, we can derive basically two kinds of models: networks of 1D models and lumped parameter ones. In this Section, we give a quick glance at their basic features, highlighting to what extent they are able to represent the behavior of the circulatory system. On this basis, we will try to give an answer to some of the questions suggested at the beginning of the Section.

The studies we present in the following paragraphs have been motivated by the “Sport and Rehabilitation Engineering Programme 2004” at the EPFL and carried out in cooperation with M. Tuveri, vascular surgeon at the S. Elena Hospital in Cagliari.

#### *Numerical models and simulations*

*1D models.* If we exploit the fact that an artery is a quasi-cylindrical vessels and that blood flows mainly in the axial direction, we build a simplified model

that ignores the transversal components of the velocity. Moreover, we could assume that the wall displaces only along the radial direction and describe the fluid-structure interaction blood flow problem in terms of the measure  $A(z, t)$  of a generic axial section  $\mathcal{A}(z)$  of the vessel (see Fig. 7, left) and the mean flux

$$Q(z, t) = \int_{\mathcal{A}(z)} \mathbf{u}_z d\sigma.$$

Here,  $z$  indicate the axial coordinate. Under simplifying yet realistic hypotheses, the following one dimensional (1D) model is obtained [FQ04]

$$\begin{aligned} \frac{\partial A}{\partial t} + \frac{\partial Q}{\partial z} &= 0, \\ \frac{\partial Q}{\partial t} + \frac{A}{\rho} \frac{\partial p}{\partial A} - \alpha \bar{\mathbf{u}}_z^2 \frac{\partial A}{\partial z} + 2\alpha \bar{\mathbf{u}}_z \frac{\partial Q}{\partial z} + K_R \left( \frac{Q}{A} \right) Q & \end{aligned} \quad (5)$$

for  $z \in (0, L)$ , and  $t > 0$ , which describes the flow of a Newtonian fluid in a compliant straight cylindrical pipe of length  $L$ . Here,  $\bar{\mathbf{u}}_z \equiv A^{-1} \int_{\mathcal{A}} \mathbf{u}_z d\sigma$ , and the parameter  $\alpha$ , called *momentum correction* or also *Coriolis coefficient*, is defined as:  $\alpha = (A \bar{\mathbf{u}}_z^2)^{-1} \int_{\mathcal{A}} \mathbf{u}_z^2 d\sigma$ . The pressure is assumed to be function of  $A$  according to a constitutive law that specifies the mechanical behavior of the vascular tissue. Different models can be obtained by choosing different pressure-area laws. Finally,  $K_R$  is a parameter accounting for the viscosity of the fluid, whose expression depends on the simplifying assumptions made (see [FQ04] and [CK02]).

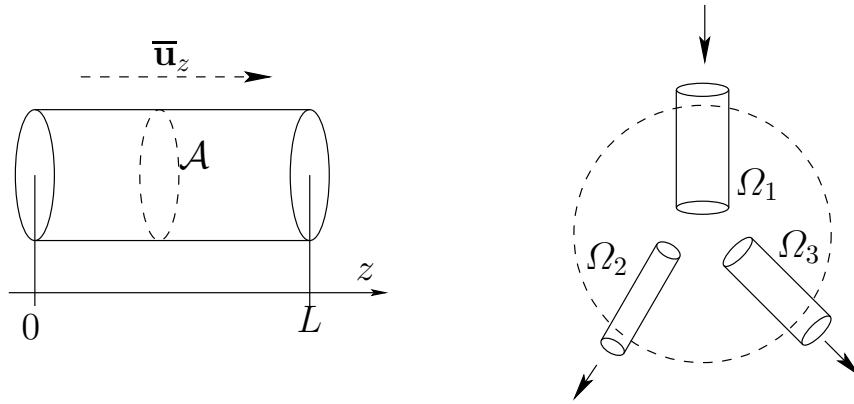


**Fig. 7.** Left: representation of an arterial cylindrical segment. Right: sketch of a bifurcation

The hyperbolic system (5) can be used to describe blood flowing in a vascular segment. Since the arterial system can in fact be assimilated to an hydraulic network, it may be modelled as a network of 1D hyperbolic PDE's

as long as suitable matching conditions are found at the branching points. If we denote by  $\Omega_1$  a proximal segment, by  $\Omega_2$  and  $\Omega_3$  the two branches (see Fig. 7, right), a possible set of conditions that ensure mass and energy conservation is [FQ04]

$$\begin{aligned} Q_1 + Q_2 + Q_3 &= 0, \\ \left(p + \frac{1}{2}|\bar{\mathbf{u}}_z|^2\right)_1 &= \left(p + \frac{1}{2}|\bar{\mathbf{u}}_z|^2\right)_2 = \left(p + \frac{1}{2}|\bar{\mathbf{u}}_z|^2\right)_3, \end{aligned} \quad (6)$$

where all quantities are computed at the bifurcation point. More sophisticated bifurcations conditions may consider also the effect of the angle among the branches (see e.g. [FLQ03]).

The system of equations formed by (5) and (6) is stable [FLQ03] and will be used in the next paragraph to model circulation. We warn the reader that research is still active in finding different 1D models that could improve the computation of the wall shear stress [RS04] or the description of curved segments [Lam04]. Furthermore, the estimation of the physical parameters of the model in order to obtain realistic computation is a rather complex task, an account is given in [MCDG05].

*Lumped parameters models.* A further simplification in the mathematical description of the circulation relies on the subdivision of the vascular system into *compartments*, according to criteria suited for the problem to hand. The blood flow, as well as the other quantities of interest, is described in each compartment by a set of parameters depending only on time. For blood flow, these parameters are the average flux and pressure in the compartment. The mathematical model is typically given by a system of ordinary differential equations in time that govern the dynamics of each compartment, and their mutual coupling. Often, these models are called *lumped parameters* models or also (with a little abuse of notation) 0D models.

In this way, large parts of the circulation (if not all) can be modeled. The level of detail can be varied according to the problem needs. For instance, if the objective is the study of the regulatory mechanism in the circle of Willis and its interaction with the global circulation, we will adopt a more detailed description of the former, while we might describe the latter with just a few compartments.

A useful way of representing lumped parameter models of the circulation is based on the analogy with electric networks. In this analogy the flow rate is represented by the electric current and the pressure by the voltage. The equations coupling the different compartments are given by the *Kirchhoff balance laws*, which state the continuity of mass and pressure. The effects on blood dynamics due to the vascular compliance is here represented by means of capacitances. Similarly, inductances and resistances represent the inertial terms and the effect of blood viscosity, respectively (see e.g. [FV03b]).

Exploiting the same analogy, it is also possible to devise a lumped parameter representation of the heart. In particular, the electric analog of each

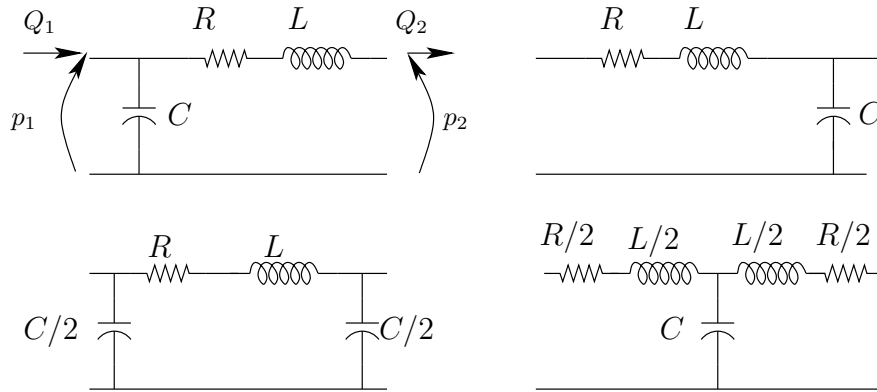


**Fig. 8.** Four possible lumped parameters representation of a compliant vessel in terms of electrical circuits. The four cases differ for the state variables and the upstream/downstream data to be prescribed

ventricle is given in Fig. 9 where the presence of heart valves has been taken into account by *diodes* which allow the current flow in one direction only. For more details about this model, see [FV03b].

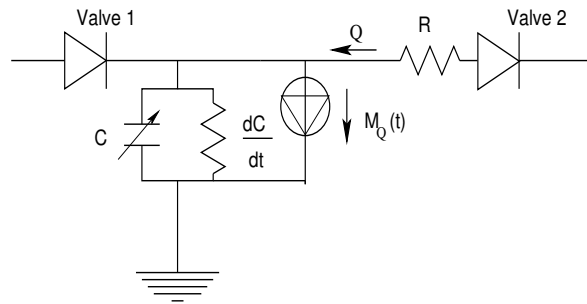


**Fig. 9.** Network for the lumped parameters modeling of a ventricle

Fig. 3 illustrates different electrical schemes that may be used to describe blood flow in a passive compartment. By coupling together these schemes and the model of the heart it is possible to derive a lumped parameter model of the whole circulatory system.

From the mathematical viewpoint, a general representation of lumped parameters models is a Differential-Algebraic-Equations (DAE) system in the form

$$\begin{cases} \frac{dy}{dt} = B(\mathbf{y}, \mathbf{z}, t) & t \in (0, T] \\ G(\mathbf{y}, \mathbf{z}) = 0 \end{cases} \quad (7)$$

supplemented with the *initial condition vector*  $\mathbf{y}|_{t=t_0} = \mathbf{y}_0$ . Here,  $\mathbf{y}$  is the vector of *state variables*, associated to the flux in an inductance and the pressure in a capacitance, while  $\mathbf{z}$  are the variables of the network which do not appear under time derivatives. Finally  $G$  represents the set of algebraic equations that come from the Kirchhoff laws. If we assume that the Jacobian matrix  $\partial G/\partial \mathbf{z}$  is non singular, by the implicit function theorem we can express  $\mathbf{z}$  as a function of  $\mathbf{y}$  and, with some additional algebraic manipulations, resort to the following reduced non-linear Cauchy problem

$$\begin{aligned} \frac{d\mathbf{y}}{dt} &= \boldsymbol{\Phi}(\mathbf{y}, t) = A(\mathbf{y}, t)\mathbf{y} + \mathbf{r}(t) \quad t \in (0, T] \\ \mathbf{y} &= \mathbf{y}_0, \quad \text{at } t = t_0. \end{aligned} \quad (8)$$

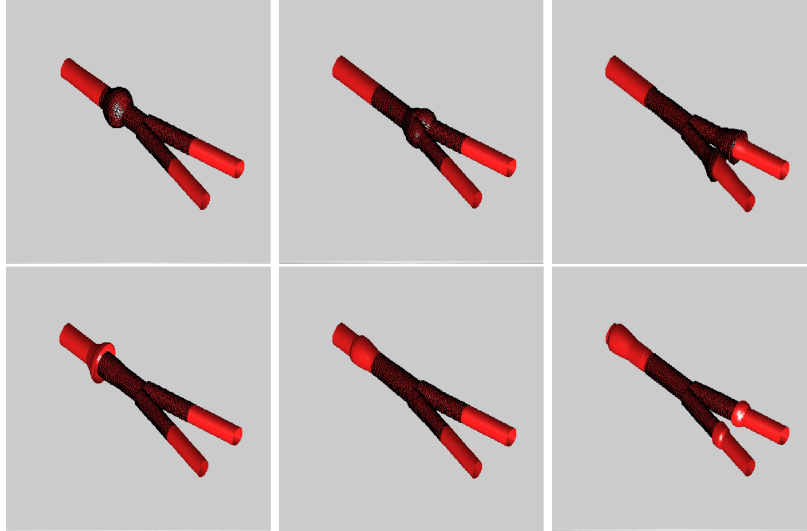


**Fig. 10.** Snapshots of the simulation of a vascular bifurcation with a prosthesis, carried out with a 1D model. The three pictures in the top row illustrate the case of a prosthesis softer than the arterial wall. The most relevant reflection is at the distal interface between the prosthesis and the vessels (right). At the bottom row the results obtained using the same boundary data but with a prosthesis stiffer than the vascular wall. The most relevant reflection is at the proximal interface between the vessel and the prosthesis (left) and it back propagates to the heart (simulations carried out by D. Lamponi)

*An example of a systemic model.* The arterial system can be considered as a transmission line where the pressure wave generated by the heart propagates to the periphery. The propagation (velocity, reflections, etc.) clearly depends on the line characteristics. This is a rather schematic picture of the basic

mechanism of "pulse wave" propagation which can aid understanding why a peripheral occlusion or an endovascular prosthesis could induce for instance an overload on the heart. As a matter of fact, the occlusion induces a wave reflection that might back-propagate along the transmission line and reach the heart.

A similar effect may be induced by a vascular prosthesis. Indeed, the replacement of a part of a diseased artery with the prosthesis corresponds to replacing a portion of the transmission line with one with different physical characteristics. This introduces a discontinuity that stimulates reflections back-propagating to the heart. One dimensional hyperbolic models of the type here described are very well suited to describe these propagation phenomena. In Fig. 10 we report some snapshots of the numerical solution obtained by simulating with 1D models the implant of a prosthesis at the abdominal bifurcation to cure an aneurysm. The pictures on the top row represents the case of an endo-prosthesis made with material softer that the vascular tissue. On the bottom, we illustrate the case where the prosthesis is stiffer. The presence of a strong back-reflection in the latter case is evident. When the reflected wave reaches the heart may induce a pressure overload. These results may guide the design of better prostheses.

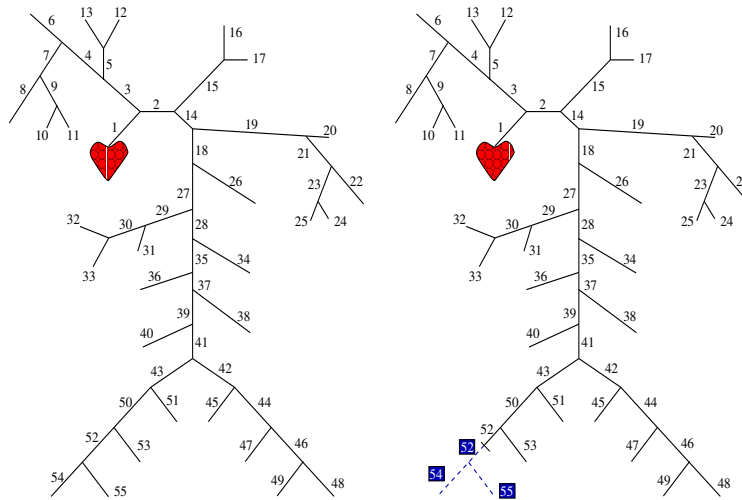


**Fig. 11.** Arterial tree composed of a set of 55 straight vessels, described by 1D models (see [WP04]). On the right a pathological case, in which some of the vessels are supposed to be completely occluded.

A more complete 1D network, like the one including the largest 55 arteries shown in Fig. 11, left, may be adopted for a more thorough numerical investi-

gation of the systemic dynamics. Since “left ventricle and arterial circulation represent two mechanical units that are joined together to form a coupled biological system” [NO90, Chap.13], we need to couple the 1D model with a model of the heart (or at least of the left ventricle), for instance a lumped parameter model. In the numerical results presented hereafter, the opening of the aortic valve is driven by the difference between the ventricular and the aortic pressure,  $P_v$  and  $P_a$ , while the closing is governed by the flux. Peripheral circulation in smaller arteries and capillaries may be accounted as well by lumped parameter models of the kind represented in Fig. 8.

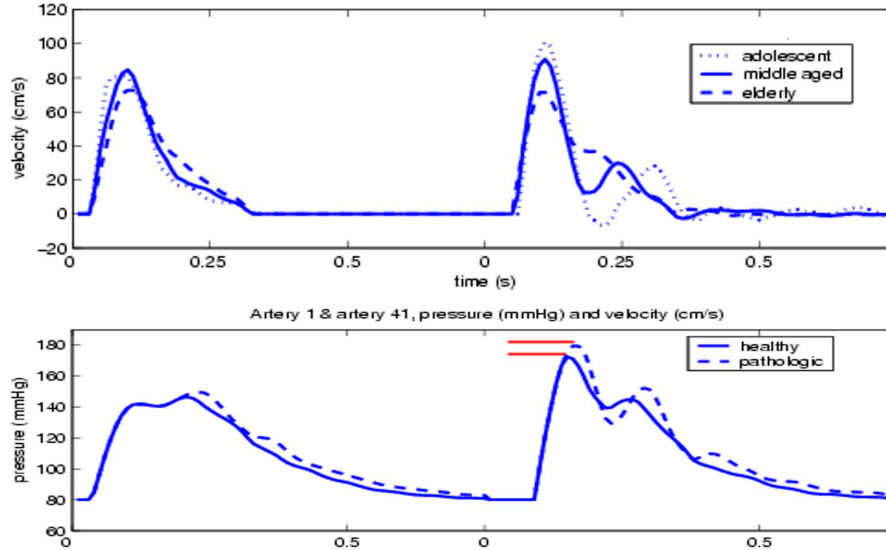


**Fig. 12.** Top: Time history of blood velocity in the thoracic aorta for different aged individuals. Bottom: Time history of the pressure in the ascending aorta for an healthy individual (solid line) and one suffering a complete occlusion of the right femoral artery (dashed)

Figure 12 (top) illustrates the behavior of the arterial pressure and flow in arteries in subjects of different age. Ageing is indirectly simulated by changing the physical characteristics of the arterial walls in the 1D model. More precisely, the stiffness of the arterial walls has been increased with age, in accord to clinical evidence. The effects are evident.

Finally, Fig. 12 (bottom) compares the results of a physiological and a pathological case. More precisely, we report the different behaviour of the pressure in the abdominal aorta when a femoral artery is occluded, for instance by a thrombus.

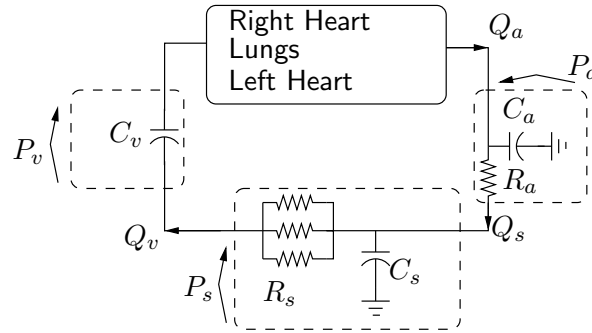


**Fig. 13.** A four compartment description of the vascular system with self-regulating controls

*Mathematical description of cardiovascular self-regulation.* So far, we have implicitly assumed that the parameters that govern our model, like resistances and compliances, are given values, obtained from measurements or by other means. This is not true, as it is well known from daily experience: the duration of the heart beat is different at rest or after a long run! The circulatory system is extremely robust, in the sense that it ensures the correct blood supply to organs and tissues in very diverse situations.

This is possible thanks to self regulating mechanisms. One of such mechanisms ensures that the arterial pressure is maintained within a physiological range (about  $90 - 100\text{mmHg}$ ). Indeed, if pressure falls below this range the oxygenation of the peripheral tissues would be gravely reduced; on the other hand, a high arterial pressure would induce vascular diseases and heart overload. This regulation system is called *baroreflex effect* and is described, for instance, in [HP92] and [KS98]. The elements of the feedback baroreceptor loop are: (i) the sets of *baroreceptors* located in the carotid arteries and the aortic arc. They transmit impulses to the brain at a rate increasing with the arterial pressure; (ii) the *parasympathetic nervous system*, which is excited by the activity of baroreceptors and can slow down the heart rate; (iii) the *sympathetic nervous system*, which is inhibited by the baroreceptors and can increase the heart rate. It controls also the venous pressure and the systemic resistance. Another ingredient of the self-regulating capabilities of the arterial system is the so called *chemoreflex effect*, a mechanism able to induce capillaries dilation and opening when an increment of oxygen supply is required by the organs, for instance during heavy exercise.

The models presented so far do not include these feedback mechanisms. Moving from the simple four-compartments scheme depicted on Fig. 13 (comprising heart and lungs, an arterial compartment, a systemic compartment and venous compartment) a possible model including the baroreflex and chemoreflex effects is described in the following paragraphs, more details are found in [D'A05].

The model is formed by different systems, mutually interacting.

1. *Haemodynamics:*

$$\begin{cases} C_a \frac{dP_a}{dt} = Q_a - \frac{P_a - P_s}{R_a} \\ C_s \frac{dP_s}{dt} = \frac{P_a - P_s}{R_a} - \frac{P_s - P_v}{R_s} \\ C_v \frac{dP_v}{dt} = Q_a - C_a \frac{dP_a}{dt} - C_s \frac{dP_s}{dt} \\ Q_a = \frac{1}{T} \left( \Delta V(P_v) - \frac{P_a}{E} \right) \end{cases} \quad (9)$$

where  $C_a, C_s$  and  $C_v$  are the arterial, systemic and venous compliances, respectively, while  $R_a, R_s$  and  $R_v$  are the corresponding resistances. In particular,  $R_s$  is given by the contribution of the skeletal muscle ( $sm$ ), the splanchnic compartment ( $sp$ ) and other organs ( $o$ ) so that  $R_s = (R_{sm}^{-1} + R_{sp}^{-1} + R_o^{-1})^{-1}$ . Finally,  $T$  is the heart beat duration,  $E$  the cardiac elastance and  $\Delta V$  the ventricular volume variation during the heart beat, which is a function of the venous pressure.

2. *Baroreceptor control:*

$$\begin{cases} \frac{dT}{dt} = f_T(T, f_B(P_a)) \\ \frac{dE}{dt} = f_E(E, f_B(P_a)) \end{cases} \quad (10)$$

where  $f_T, f_E$  and  $f_B$  are suitably defined non-linear functions. In particular  $f_B$  describes the action of the baroreceptor loop.

3. *Chemoreflex control:*

$$\begin{cases} \frac{d\tilde{R}_i}{dt} = f_i(\tilde{R}_i, f_B(P_a)) & i \in (sm, p, o) \\ \frac{d\tilde{x}}{dt} = f_{x_i}(x_i, f_C(c_{oxy,i})) \\ R_{sm} = \frac{\tilde{R}_{sm}}{1 + x_{sm}}, \quad R_{sp} = \tilde{R}_{sp}(1 + x_{sp}), \quad R_o = \frac{\tilde{R}_o}{1 + x_o} \end{cases} \quad (11)$$

where  $c_{oxy,i}$  is the oxygen concentration in compartment  $i$  ( $i = sm, sp, o$ ).

4. *Metabolism:* The oxygen concentration will in turn be given by a model for the tissue metabolism, possibly including the reaction with other chemicals. If  $\mathbf{c}_i$  denotes the vector of chemical concentrations in compartment  $i$ , a general formulation of this model reads

$$\frac{d\mathbf{c}_i}{dt} = \mathbf{A}_i \mathbf{c}_i + Q_i (\mathbf{c}_a - \mathbf{c}_i) \quad (12)$$

where  $\mathbf{A}_i$  is the *stoichiometric matrix* describing the interactions among chemicals in the compartment, and the second term in the right hand side is a *transport term*.

A main concern in devising this kind of models is the identification and tuning of all the parameters appearing in the equations [D'A05]. Often, they have to be inferred by indirect measurements and observations.

Despite of its apparent simplicity, this model is able to simulate different realistic situations, which are the virtual counterpart of actual protocols in sport medicine and physiology. For instance, in Fig. 14 we illustrate the time evolution of the haemodynamic variables during an incremental exercise with a linearly increasing workload and a total duration of 10 minutes. An extensive validation of this kind of models is the subject of current research.

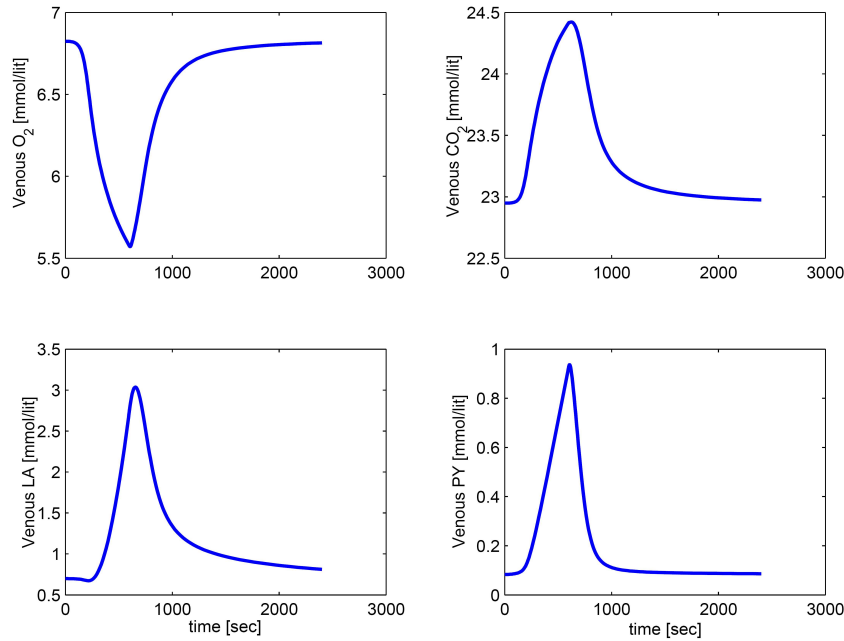


**Fig. 14.** Time history of haemodynamics variables in an individual under an incremental 10 minutes exercise with a linearly increasing workload (courtesy of C. D'Angelo)

### 2.3 The Design of Drug Eluting Stents

#### *The problem*

The treatment of coronary pathologies in an advanced stage or the cure of stenosis caused atherosclerotic plaques may be carried out by the implant of

a *stent*. The stent is a microstructure, which is formed by interwoven and adequately shaped metal filaments. It is driven inside the arterial system until it is near the arteriosclerotic plaque. Then it is expanded to bring the arterial lumen to the original diameter and restore an adequate blood flow. Generally, these medical devices are permanently left on the implantation. The implant of a stent is a less invasive procedure than bypass surgery and therefore its adoption by vascular surgeon is increasing. Data extracted from the Association Heart Diseases and Stroke Statistics 2004 confirm that since 1979 to 2001 the number of stent implants in the United States has tripled, and about 1,208,000 of such operations were performed just in 2001.

Cardiovascular stents have to meet many requirements, which are at times in contrast with each other. For example, they must be extremely flexible along their longitudinal axis in order to be able to find their way through contorted arteries and reduced diameters. They must be adequately visible with X-ray techniques, since the implant is guided from the outside. When they are driven through the arterial system they are in a compressed state, and their radial dimension is minimal. Yet, they must expand easily to their original size once the final position has been reached. Furthermore, they should have enough stiffness to maintain the final expanded shape under the mechanical strain exercised by the atherosclerotic plaque and the vessel wall. Last, but not least, they must be biocompatible to minimize thrombogenesis.

The study of the impact of a stent implant on the blood flow, both locally and in the whole cardiovascular system, is an extremely complex problem and mathematical models can be of assistance. As we have pointed out in the previous Section, an implant that increases the rigidity of the vascular wall will reflect back the part of energy of the flow and could generate in some cases an increase in the peak pressure in the proximal region and possibly an overload of the heart. However, in the case of a stent there is a second, perhaps more important source of disturbances, namely the interaction with the cells of the vessel wall in the contact region. Metals like iron and nickel, which are used to manufacture certain families of stents, can interact with the cells of the endothelium, the tunica intima and media, causing an inflammatory reaction which can lead to the uncontrolled proliferation of smooth muscle cells, yielding a narrowing of the vessel lumen. To contrast this event biomedical researchers have developed stents coated with a microlayer of material designed to store an anti-inflammatory drug which is slowly released into the vessel wall tissue. Here, the most relevant points are the choice of the drug and the design of a suitable matrix that can store and release the anti-inflammatory agent with the correct rate. The latter point calls for the development of new nanostructured materials and technologies to store the drug into them.

A numerical simulation of the release of drug into the arterial tissue require the development of this pharmacokinetic models, to be coupled with transport-diffusion equations. Numerical computations will enable to test sev-

eral design configurations of the stent, and help to select the most appropriate one. For more details, see [Zun04].

This research is currently developed in cooperation with the Laboratory for Biological Structures (LABS) of Politecnico di Milano, the Department of Structural, Environmental and Biological Chemistry of the University of Bologna, the CMCS Centre of the EPFL, Lausanne and the Service de Chirurgie Cardio-Vasculaire, Centre Hospitalier Universitaire Vaudois (CHUV) in Lausanne.

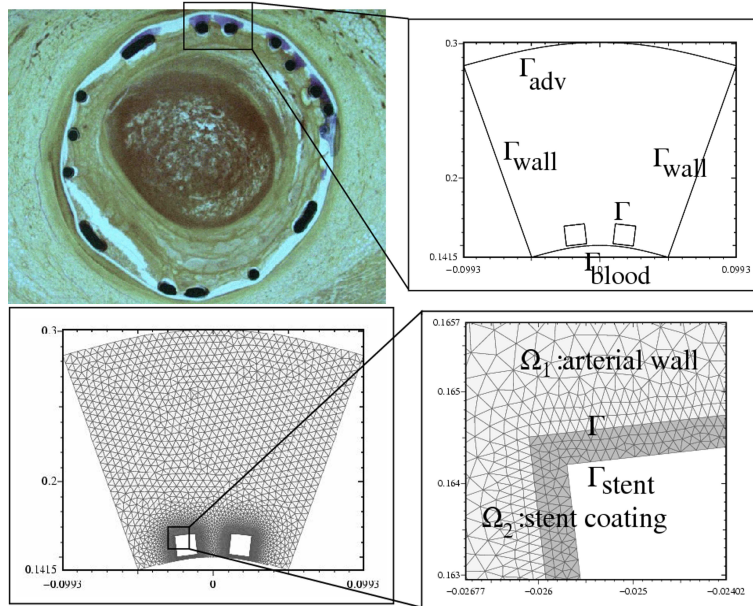


**Fig. 15.** Detail of a stented artery, with the representation of the domain used for the numerical simulation of the stent design problem, and the associated computational mesh (courtesy of P. Zunino)

*Numerical models and simulations*

Following [Zun04], we assume that the tissues constituting the arterial walls, as well as the stent coating, behave as porous media with respect to the filtration of plasma and the transfer of molecules[Fry87, RP96]. For the sake of simplicity, we will consider here only the interaction of the stent with the media, which is the thickest tissue layer constituting the arterial wall, and we assume that the stent is completely embedded into the wall (see 15). The domain of the problem will be therefore given by two subdomains, the media and the stent coating, where the filtration of plasma and the diffusion, transport and chemical binding of the drug have to be modelled.

*Models and Methods.* We denote with subscript 1 the quantities related to the media and with subscript 2 the quantities related to the coating of the stent. The portion of the wall will be therefore denoted by  $\Omega_1$ , while  $\Omega_2$  represents the considered portion of the stent, as shown in Figure 15. The interface  $\Gamma$  between  $\Omega_1$  and  $\Omega_2$  can be seen as a boundary for the governing equations on  $\Omega_1$  and  $\Omega_2$ , respectively. Let moreover  $\Gamma_{blood}$  be the boundary separating the arterial wall from the arterial lumen and  $\Gamma_{adv}$  that separating the wall from the outer tissues, the latter corresponding to the surface of the adventitia. We denote by  $\mathbf{u}_1$  the volume averaged filtration velocity of the plasma in the media. The velocity  $\mathbf{u}_1$  is governed by the Darcy equation,

$$\begin{cases} \mathbf{u}_1 = -\frac{K_1}{\mu_1} \nabla p_1 \text{ with } \nabla \cdot \mathbf{u}_1 = 0 \text{ in } \Omega_1, \\ p_1 = p_{blood} \text{ on } \Gamma_{blood}, \quad p_1 = p_{adv} \text{ on } \Gamma_{adv}, \quad \mathbf{u}_1 \cdot \mathbf{n}_1 = 0 \text{ on } \Gamma \cup \Gamma_{wall}, \end{cases} \quad (13)$$

where  $\mathbf{n}_1$  and  $\mathbf{n}_2$  are the outward normal vectors with respect to  $\partial\Omega_1$  and  $\partial\Omega_2$ , respectively. Moreover, in equation (13),  $K_1$  is the Darcy's permeability of the media, while  $\mu_1$  is the viscosity of plasma.

As for the chemical dynamics, we are interested in the volume averaged concentration in each domain,  $c_i$  ( $i = 1, 2$ ), including the amount of drug present in the fluid and the one bound with the tissue. These concentrations satisfy the equations

$$\begin{cases} \frac{\partial c_1}{\partial t} + \nabla \cdot (-D_1 \nabla c_1) + \frac{\gamma \mathbf{u}_1 c_1}{k_1 \epsilon_1} = 0, & \text{in } \Omega_1, \\ c_1 = 0 \text{ on } \Gamma_{blood}, \\ -D_1 \nabla c_1 \cdot \mathbf{n}_1 = 0 \text{ on } \Gamma_{adv} \cup \Gamma_{wall}. \end{cases} \quad (14a)$$

and

$$\begin{cases} \frac{\partial c_2}{\partial t} + \nabla \cdot (-D_2 \nabla c_2) = 0, & \text{in } \Omega_2, \\ -D_2 \nabla c_2 \cdot \mathbf{n}_2 = 0 \text{ on } \Gamma_{stent}. \end{cases} \quad (14b)$$

Here, the parameters  $D_1$  and  $D_2$  represent the diffusivities of the considered drug in the media and in the stent coating, respectively,  $k_i$  is the so-called partition coefficient of the drug, and  $\epsilon_i$  is the porosity of the media. The coefficient  $\gamma$  accounts for possible frictional effects between the molecules of drug and the pores of the arterial walls. The boundary condition on  $\Gamma_{blood}$  reflects the assumption that the concentration of the drug in the blood is negligible, while the one on  $\Gamma_{adv}$  states that the diffusive flux on this boundary is vanishing. The same condition is applied to  $\Gamma_{wall}$  by virtue of the axial symmetry of the domain  $\Omega_1$ .

The equations (14a) and (14b) should be coupled by a suitable set of matching conditions. This is a delicate issue: in fact, the physical properties of the arterial walls with respect to mass transfer are very different from those of the stent coating, where the drug is initially stored, and this can induce strong variations in the drug concentration when passing from one medium to

the other. The region at the interface is a permeable membrane that accounts for possible jumps of the concentrations on its sides. Matching conditions can be derived from the so-called Kedelm-Katchalsky model (see [KK58]), which enforces the mass conservation across the subdomains interface:

$$\begin{cases} -D_1 \nabla c_1 \cdot \mathbf{n}_1 = D_2 \nabla c_2 \cdot \mathbf{n}_2, \\ -D_1 \nabla c_1 \cdot \mathbf{n}_1 = \sigma(c_1/k_1\epsilon_1 - c_2/k_2\epsilon_2), \end{cases} \quad \text{on } \Gamma \quad (15)$$

where  $\sigma$  is the membrane permeability.

In this model the drug dynamics does not affect the plasma flow, so we can solve (13) independently of the concentration problem, yielding a simplification of the numerical scheme as well. For a discussion and analysis of the previous model, we refer to [QVZ02b] and [QVZ02a] where finite elements were used for the space discretization and an implicit Euler scheme for the time discretization. The application of this technique yields at every time step a system of linear algebraic equations featuring a block structure that reflects the multidomain nature of the problem. The strongly heterogeneous nature of the two subdomains is reflected in the bad conditioning properties of such a matrix, so that specific techniques have to be adopted for its numerical solution. A possible approach is to resort to the domain decomposition method applied to the multidomain structure of the problem (see [QV99]). In [QVZ02a] this technique was used to precondition a GMRes iterative method, obtaining optimal convergence properties. In particular, it is shown that the preconditioner has the same spectral properties of the matrix governing the problem.

*Results.* The drug release by the stent coating is influenced by many factors, namely the shape of the fibers and the coating, the properties of the drug and that of the arterial wall. Numerical simulations enable the evaluation of the behavior of various configurations highlighting the most effective technological solutions (see [Zun04]). In Fig. 16 we illustrate some numerical results obtained from the simulation of a *programmable stent*. In particular, in the top-left picture we illustrate the evolution in time of the drug concentration (normalized with respect to the concentration at the initial instant) in the stent coating, in the vascular wall and the sum of the two curves. Part of the drug is lost in the blood flow and this explains the reduction in time of the total amount of drug. In the other pictures we show the iso-lines of concentration after one (top, right), two (bottom, left) and three (bottom, right) days respectively.

The profile of the drug release rate is a key factor for the design of a drug eluting stent. Numerical simulations of this kind may help to choose the most appropriate drug components or the best coating matrix characteristics. In particular, from Fig. 16 we conclude that coffee-cup stents seem to ensure a slow drug release over three days.

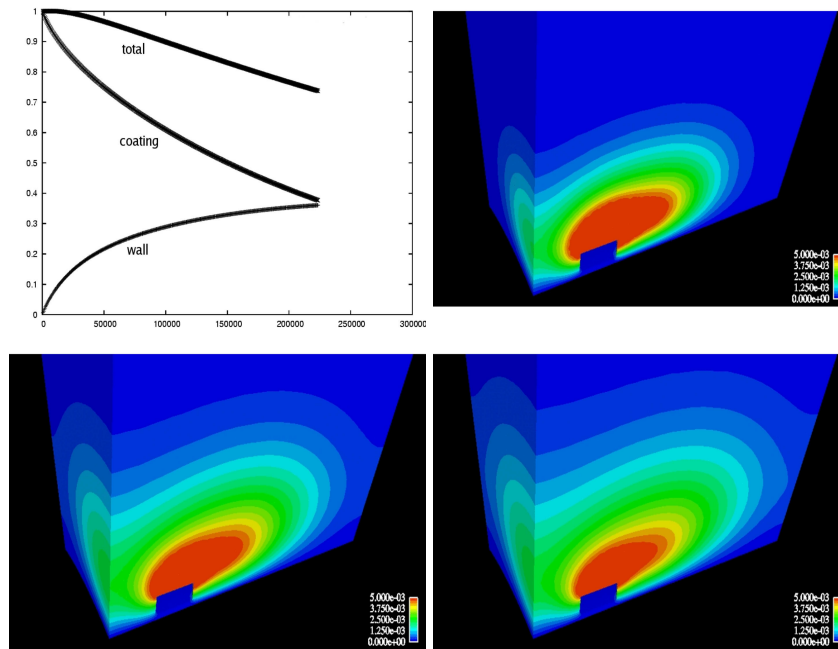


**Fig. 16.** Coffee-cup stents simulation. Top, Left: Drug (heparin) concentration evolution in time in the coating and in the wall. Top, Right: Concentration iso-lines after 1 day. Bottom, Left: after 2 days. Bottom, Right: after 3 days (courtesy of M. Prosi)

## 2.4 Pulmonary and systemic circulation in individuals with congenital heart defects

### *The problem*

Some serious congenital heart anomalies feature a marked hypoplasia of the left heart, including the aorta, aortic valve, left ventricle and mitral valve. These pathologies are indicated with the name of *Hypoplastic Left Heart Syndrome* (HLHS) and need to be treated surgically. A possible approach is based on a staged reconstruction involving three operative procedures (see [Nor91, Bov98]). At the first stage, called *Norwood procedure*, the main pulmonary trunk is attached to the augmented aorta to establish an unobstructed systemic circulation. An interposition graft called *systemic-to-pulmonary artery shunt* (diameter 3, 3.5 or 4 mm) is placed to provide pulmonary perfusion and gas exchange. Two possible options for this stage are the central shunt (CS) and the right modified Blalock-Taussig shunt (MBTS). In the former, a by-pass is placed directly between the aorta and the pulmonary artery, while in the MBTS the conduit is interposed between the innominate

artery and the pulmonary artery (see Fig. 17). At the subsequent stages, pulmonary perfusion is achieved by connecting the superior vena cava (second stage) and the inferior vena cava (third stage) directly to the pulmonary artery. The systemic-to-pulmonary shunt is removed at the second stage. In some cases, this intervention has induced coronary insufficiency, for reasons that are not completely understood, and, in particular, the influence of shunt position and diameter on systemic hemodynamics is not clear.

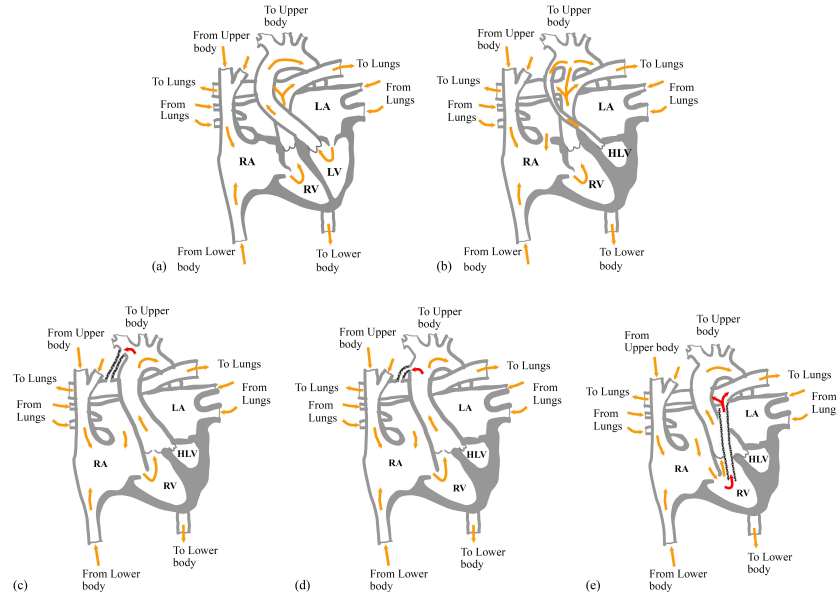


**Fig. 17.** Top Left: Normal heart, Top Right: Hypoplastic left ventricle. Bottom Left: Modified Blalock-Taussig Shunt. Bottom Middle: Central-Shunt. Bottom Right: Sano operation (courtesy of F. Migliavacca)

Another surgical approach has been recently proposed by Sano in [SIK<sup>+</sup>03] as a replacement of the Norwood procedure, and will be hereafter referred to as *the Sano operation* (SO). It consists mainly in the connection of the systemic circulation to the pulmonary one by means of a synthetic vessel, whose diameter typically ranges from 4 to 6 mm, connecting the right ventricle to the pulmonary arteries (see Fig. 17). This alternative seems to have many potential advantages. In particular, diastolic coronary perfusion may be more stable. However, many questions are still open concerning, for instance, the optimal shunt size and shunt material, the growth and distortion of the pulmonary arteries, possible ventricular volume overload due to shunt backward flow, and potential risk of arrhythmia.

Mathematical models and numerical simulations can help to understand the problem, provide quantitative data for comparing the different options, and eventually support the decisions of the surgeon. A crucial breakthrough for the correct simulation of this problem has been the *geometrical multiscale approach*. This moves from the consideration that, on the one hand we need to have an accurate simulation of the local haemodynamics in order to investigate the influence of the different possible shunt options and the possible presence of backward flow. On the other hand, it is crucial to analyze the mutual influence of the local haemodynamics on the systemic one and, for instance, to assess to which extent coronary perfusion is affected by the presence of the shunt. As we have pointed out in Sect. 1, numerical models of these type demand for specific techniques that we will briefly illustrate in the next sections. For more details see [LDM<sup>+</sup>02, FV03b, FV05]. Numerical results on the Norwood procedure and the Sano operation are taken from [LBM<sup>+</sup>05] and [MBP<sup>+</sup>05].

This research has been developed in cooperation with the Laboratory for Biological Structures at the Politecnico di Milano with the partnership of the Cardiothoracic Unit of the Great Ormond Street Hospital in London and the Section of Cardiac Surgery, The University of Michigan School of Medicine, in Ann Arbor, Michigan, Usa.

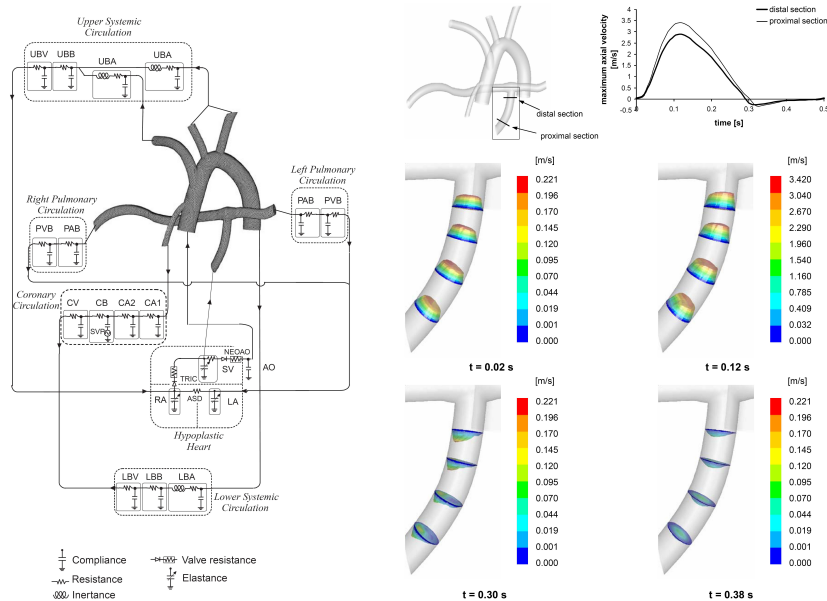


**Fig. 18.** Left: Geometrical multiscale model of the Sano Operation which couples a detailed model of the shunt and a lumped parameters representation of the circulation. Right: Flow profiles in the shunt of the Sano Operation (courtesy of F. Migliavacca)

*Numerical models and simulations*

A possible approach to account for both local and systemic dynamics is to couple the Navier-Stokes equations in the domain of interest, the shunt and its neighborhood, with simplified models like the ones introduced in Sect. 2.2 for the description of the remainder of the circulatory system. A diagram of the model obtained in this way in the case of the Sano Operation shunt is shown in the left picture of Fig. 18. At the mathematical level, this model implies the coupling between partial and ordinary differential equations. For their numerical solution, it is then natural to resort to an iterative approach based on the splitting of the whole problem into its basic components. A schematic representation of a possible numerical approach is given in Fig. 19. An explicit scheme is used for the lumped parameters model to advance time from time level  $t^n$  to  $t^{n+1}$ . The computed pressures on the interface are then imposed as boundary conditions for solving the Navier-Stokes problem, advanced in time by an implicit scheme.

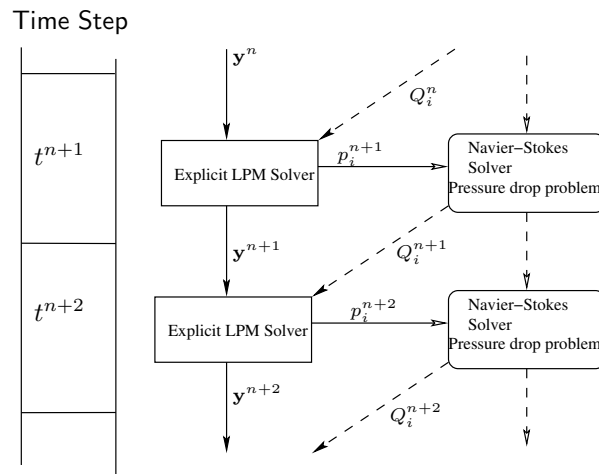


**Fig. 19.** Possible numerical scheme for the coupling of a Lumped Parameter Model (LPM) and the Navier-Stokes problem

We may observe that the pressures provided by the lumped parameter models at the interface are in fact average quantities. Therefore, the Navier-Stokes subproblem requires to solve equations (1) with the following interface boundary conditions

$$\frac{1}{\text{meas}(\Gamma_i)} \int_{\Gamma_i} p ds = P_i(t), \quad i = 1, 2, \dots, m \quad (16)$$

where  $m$  is the number of interfaces between the local and the systemic sub-problems. In Fig. 18, for instance, we have  $m = 8$ . This initial-boundary

value problem is not complete, since the Navier-Stokes problem would require pointwise boundary data. This mismatch can be overcome by completing the defective data given by the systemic submodel. One task of the geometrical multiscale approach is to minimize the numerical artifacts introduced by this completion.

In [HRT96] a particular *weak or variational formulation of the boundary problem* has been devised which allows to fulfill conditions (16), giving rise to a well-posed problem. In fact, this formulation implicitly forces natural (Neumann-like) boundary conditions which select one particular solution among all the possible ones. A well posedness analysis of the multiscale model obtained in this way can be found in [QV03]. Depending on the specific choice of the hydraulic network representing the circulatory system in the lumped model, different “defective” boundary conditions could be prescribed for the Navier-Stokes problem on the interfaces. In particular, we may have *flow rate boundary conditions*, corresponding to impose

$$\int_{\Gamma_i} \mathbf{u}(t) \cdot \mathbf{n} \, ds = Q_i(t), \text{ for } i = 0, \dots, n. \quad (17)$$

In principle, also for these conditions we may find a suitable variational formulation that ensure the existence of a solution, but it requires to use non standard functional spaces which make the finite elements discretization somehow problematic. For this reason, a reformulation of the problem been proposed in [FGNQ02] which is more suited for the numerical approximation.

### Results

Extensive numerical simulations and comparisons with available clinical data have been carried out in [LBM<sup>+</sup>05, MBP<sup>+</sup>05].

Clinical evidence and numerical results agree in showing that the cardiac output is higher in the Norwood procedure (with both CS and MBTS approach) than with the SO when the size of the shunt is the same (see Fig. 20 top, left). It is therefore worth comparing the different techniques for a similar value of the cardiac output, that means for example MBTS or CS with a 3mm shunt versus SO with a 4mm shunt and so on. By doing so the numerical results show that SO features a lower pulmonary flow and higher coronary perfusion and pressure with respect to the corresponding Norwood procedures (Fig. 20, top right, bottom left and bottom right). This is consistent with clinical evidence. Also the minimal, clinically irrelevant, presence of backward fluxes in the SO shunt highlighted in Fig. 18 is in agreement with the available data.

It is worth pointing out that this good agreement between numerical and clinical results has been obtained only thanks to the development of the multiscale techniques. Quoting [MBP<sup>+</sup>05]: “the use of simpler, stand-alone 3-D or lumped parameter models would not yield results as meaningful as those

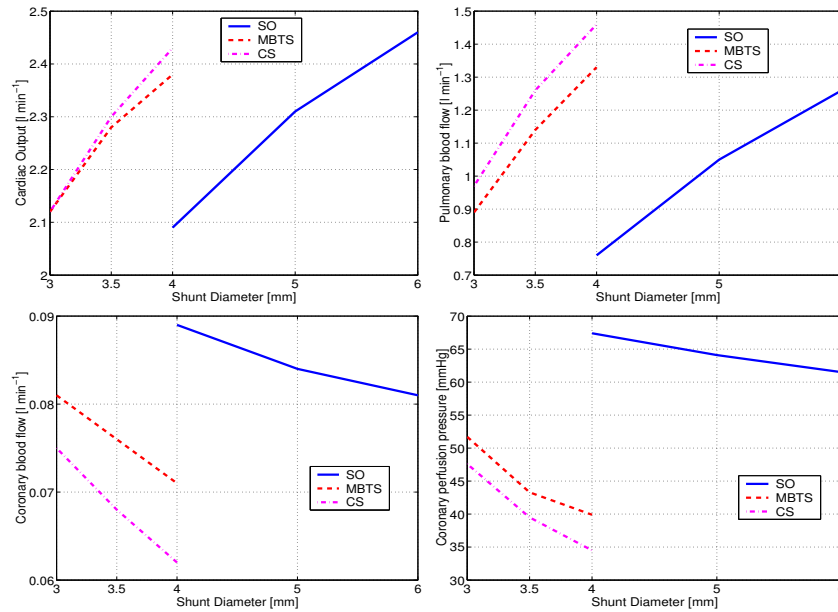


**Fig. 20.** Comparison among MBTS,CS, and SO with shunt sizes ensuring comparable cardiac output (top, left): pulmonary blood flow (top, right), coronary flow (bottom, left) and pressure (bottom, right) (courtesy of F. Migliavacca)

obtained here. Indeed, the adopted approach allows one to evaluate quantitatively the post-operative situation, thus suggesting its use as a tool for preoperative planning”.

## 2.5 Peritoneal dialysis optimization

### *The problem*

Chronic Kidney Disease (CKD) affects approximately 17 million Americans and about 400000 of them are either on dialysis or require kidney transplant ([ASON05]). To support End Stage Renal Disease (ESRD) patients amounts to an approximate cost of 13.82 billion dollars annually. Peritoneal dialysis (PD) occupies a well established place among the therapeutic options for patients with ESRD [MP79], [OLG04]. With this technique, blood purification is obtained by the exchange of chemicals between blood and a solution injected in the peritoneal cavity. The solution in the peritoneal cavity is periodically replaced by injections or extractions from the patient, through an external pump. The exchange of chemicals takes place across the net of capillaries permeating the peritoneum (see Fig. 21).

However, this technique sometimes can fail, essentially because of alterations in the peritoneal membrane transport characteristics leading to an inefficient small solute and/or water removal (see [GBPD<sup>+</sup>02]). The effectiveness

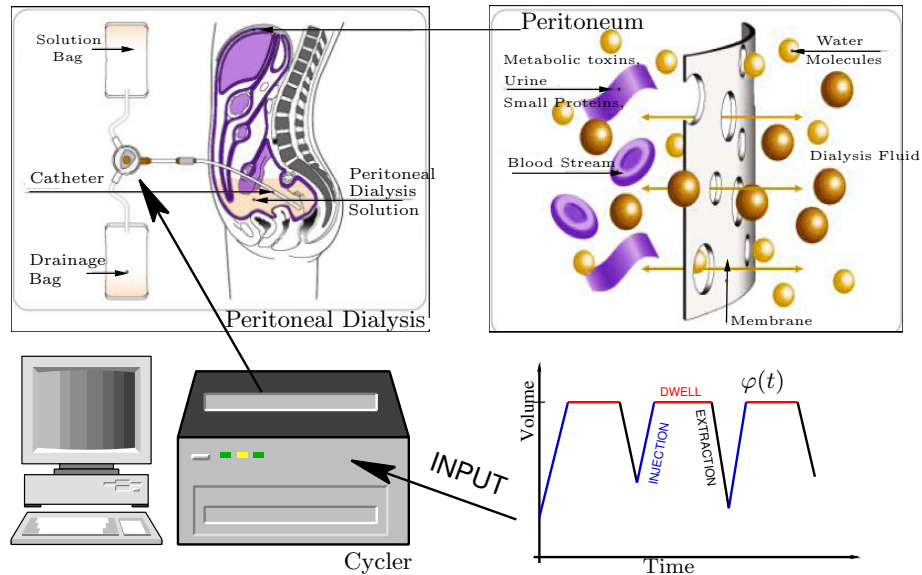


**Fig. 21.** Schematic representation of the peritoneal dialysis process: the cyclor drives the injection-dwell-extraction profile  $\varphi$  of the solution injected into the peritoneal cavity

of the therapy is directly related to the dynamics of the injection/extraction of the solution, as well as to the individual characteristics of the patient. However, often *standard therapies*, i.e. injection/extraction profiles, like CAPD (Continuous Ambulatory Peritoneal Dialysis), CCPD (Continuous Cycling Peritoneal Dialysis), TPD (tidal peritoneal dialysis), and NPD (nocturnal peritoneal dialysis) have been adopted with only an incomplete characterization of the patient. The *Dynamic peritoneal dialysis (DPD)* we are going to describe represents an alternative that customize the therapy for a specific patient by making it more efficient and/or more biocompatible. The main difficulty in the development of APD is the complexity of its prescriptions and set-up. Mathematical models allow to optimize PD therapies and facilitate the use of more elaborated therapeutic options. The final goal is to develop a procedure able to find for each patient the injections/extractions patterns that ensure the best blood purification and water removal. These tools are based on classical models proposed in the literature (see e.g. [VLMF91] and [Rip92]), derived from equations describing exchanges of chemical species across a membrane separating two solutions with different concentrations. This mathematical framework has been validated and tuned for different patients categories, in particular different characteristics of the peritoneal membrane [ZMQ<sup>+</sup>05].

This simulation environment is the result of a fruitful multi-disciplinary collaboration among a med-tech company (Debiotech s.a., Lausanne) and clin-

ical partners (Inselspital, Bern, Gent University Hospital and Ospedale le Molinette, Torino).

### *Numerical models and simulations*

*The model.* During PD therapy, the exchange of chemicals takes place through the net of capillaries within the folded peritoneal membrane. The geometrical modeling of the domain to account for spatial variations would be extremely difficult and computationally expensive. Moreover the exchanges are very rapid, due to the high concentration difference between the two sides of the membrane. Furthermore, we are mainly interested in the variation of global quantities and not in the local details. Consequently a *lumped parameters model* which describes the kinetics of chemicals during the therapy looks most suitable to this specific study. Two compartments are considered, one accounting for the body (denoted by the index  $b$ ), and one for the peritoneal cavity of the patient (denoted by  $d$ ). The latter compartment is filled by a solution of  $N$  chemicals, denoted by the indexes  $i = 1, 2, \dots, N$ . Apart from the boundary layer near the membrane, which will be accounted for by the interface condition, the concentrations may be assumed to be uniform in each compartment. The physical quantities of interest are then the *volume of the solution* and the *total amount of each solute* in the two compartments, namely  $V_b, V_d, V_b c_{b,i}, V_d c_{d,i}$ , where  $c_{b,i}, c_{d,i}$  for  $i = 1, 2, \dots, N$  are the concentrations (mass of solute per volume of solution). The interaction between the two compartments is governed by the equations prescribing the flux of solvent  $J_v$  and of each solute  $J_{s,i}$  across the membrane. In the Kedem-Katchalsky model (see [KK58]) introduced in Sect. 2.3, the membrane is characterized by a set of pores that allow the exchange of the solvent and the solutes between the two compartments. The pores are subdivided in different classes, denoted by the index  $j = 1, \dots, M$ , depending on their size. We denote by  $L_p S_j$  and  $PS_{i,j}$ , the hydraulic conductivity and permeability of the membrane relative to the  $i^{th}$  molecule through the set of pores indexed by  $j$ . Moreover  $\sigma_{i,j}$  denotes the *reflection coefficient* of the solute  $i$  with respect to the pore of class  $j$ . From the *Starling law of filtration* [KS98] we have that:

$$J_{v,j} = L_p S_j \left( \Delta p - \sum_{i=1, \dots, N} \sigma_{i,j} \Delta \pi_i \right) \quad (18)$$

where  $\Delta p$  and  $\Delta \pi_i$  ( $i = 1, \dots, N$ ) are the static and osmotic pressure differences between the two compartments respectively. In particular,  $\Delta \pi_i$  depends on the solute concentration on the two sides of the membrane, according to the *Van't Hoff law*:

$$\Delta \pi_i = RT (c_{b,i} - c_{d,i}),$$

where  $R$  is the gas constant and  $T$  is the absolute temperature. The volumes of solute in the two compartments are therefore governed by the following system of ordinary differential equations,

$$\frac{dV_d}{dt} = Q + \sum_{j=1}^M J_{v,j} + J_{v,lymph}, \quad \frac{dV_b}{dt} = - \sum_{j=1}^M J_{v,j} + J_{v,lymph} \quad (19)$$

where  $J_{v,lymph}$  is the flux of the lymphatic liquid and  $Q$  is the injection-extraction profile executed by the pump (corresponding to the time derivative of the time-volume curve depicted in Fig 21). The condition  $Q(t) > 0$  corresponds to the *injection phase* while  $Q(t) < 0$  corresponds to the *extraction phase*. Finally,  $Q(t) = 0$  corresponds to the *dwell phase*, when the liquid is left inside the peritoneal cavity. From now on we set  $\varphi(t) = \int_{t_0}^t Q(\tau) d\tau$ . In practice,  $\varphi(t)$  will be characterized by a suitably small number of parameters.

The solute flux  $J_{s,i}$  (see [Cur84], [GN84]) is the sum of a diffusive term, depending on the jump of concentration across the membrane, and a transport term, defined as the product of effective solvent flux and the average concentration within the membrane,

$$J_{s,i} = \sum_{j=1, \dots, M} [PS_{i,j} (c_{b,i} - c_{d,i}) + J_{v,j} (1 - \sigma_{i,j}) (w_i c_{b,i} + (1 - w_i) c_{d,i})], \quad (20)$$

so that

$$\begin{cases} \frac{d(V_b c_{b,i})}{dt} = g_i - J_{s,i} \\ \frac{d(V_d c_{d,i})}{dt} = J_{s,i} + Q c_{d,i}. \end{cases} \quad (21)$$

Here  $g_i$  represents the metabolic contribution to the  $i^{th}$  solute. Equations (19) and (21) provide a system of  $2N + 2$  nonlinear equations that describe the rate of change of the unknowns  $V_b, V_d, V_b c_{b,i}$ , and  $V_d c_{d,i}$ .

It is worth pointing out that this model can be applied to a large number of chemical species, with very weak limitations. In particular, it takes into account the basic chemicals considered in dialysis, as *urea*, *glucose* and *creatinine*. Furthermore, it can also be applied to *sodium*, in order to study its removal, or to *large polymers*, which are nowadays becoming an alternative for glucose to drive water outside patients with more severe kidney inefficiency.

Moreover, the model can account for different models of the peritoneal membrane, in particular the *iso-pore model* ( $M = 1$ ) and the *three-pore model* ( $M = 3$ ), where medium-sized and large pores account for large molecules (e.g. proteins) dynamics, and ultra-small pores account for the exchange of water.

From the numerical viewpoint, we have to solve an ordinary differential system. This can be done in different ways (for a general introduction see [QSS02]). However, because of the succession of injection-dwell-extraction phases, the dynamics of the process is more critical during the periods of injection and extraction, requiring in this phases a more accurate time discretization than during the dwell phase. For this reason, *adaptive time discretization methods* have been studied to balance the need of accuracy and low computational costs.

*Results.* In order to determine the efficiency of a therapy, clinicians mostly focus on two molecules, urea and creatinine, and to the net amount of fluid extracted during a therapy, the so called *ultra-filtration*. Consequently, an effective therapy is characterized by a suitable balance of the following indicators:

1. the normalized extracted urea over a week  $KT/V_{urea}$ ,
2. the creatinine clearance  $Cl_{creat}$ ,
3. the ultrafiltration  $UF$ .

We define the *efficacy parameter*  $\eta$  as a weighted combination of the previous indicators,

$$\eta = w_1KT/V_{urea} + w_2Cl_{creat} + w_3UF,$$

where  $w_1$ ,  $w_2$  and  $w_3$  are suitable weighing coefficients satisfying  $w_1 + w_2 + w_3 = 1$ . Additional factors can be hold to evaluate the adequacy of PD, such as the amount of glucose and sodium that are exchanged during therapy can be introduced as well.

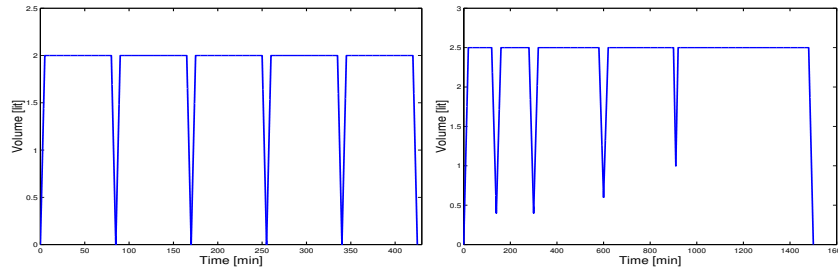


**Fig. 22.** Different possible patterns  $\varphi$  of the injection-dwell-extraction dynamics. On the left the case of a standard therapy, on the right a profile computed after optimization (courtesy of D. Mastalli)

Each therapy features a particular injection/extraction pattern  $\varphi(t)$ . In Fig. 22 we illustrate two possible therapies. Typically, the following constraints on the injection-dwell-extraction pattern has to be fulfilled:

1. the total duration  $T_{tot}$  of the therapy must not be exceeded; a typical range is 4-10 hours;
2. the total amount of dialysate  $V_{tot}$  must be fully exploited; a realistic range is 4-16 liters;
3. the peritoneal cavity should be emptied at the end of the therapy.

By means of the numerical simulations, the efficacy of a therapy can be computed for several values of the inputs. The data resulting from the numerical simulations are summarized in Figure 23, which describes the trend

of  $KT/V_{urea}$  and sodium removal for a specific patient. In particular, the picture shows that, as expected, an increase of the therapy duration or of the volume cause an increase of the  $KT/V_{urea}$  index, and that a therapy of just 5 hours cannot achieve a sodium removal greater than about  $1.5g$ . These results

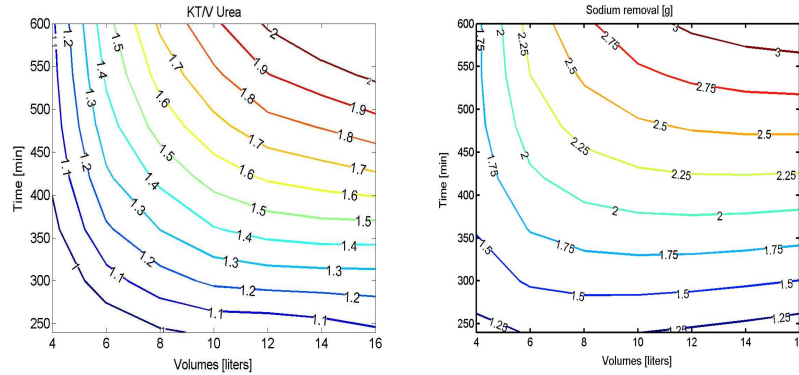


**Fig. 23.** Simulation of the peritoneal dialysis for a given patient:  $KT/V_{urea}$  (left) and sodium removal (right) as functions of the therapy time and the dialysate volume (courtesy of D. Mastalli)

on the therapy performance on a specific patient basis can help to set up an appropriate PD treatment. The final goal is the automatic determination of the injection-extraction pattern  $\varphi(t)$  able to fulfill the given requirements for each patient, and prescribed it by setting the cyclers that executes the therapy. This new framework is called DPD (*Dynamic Peritoneal Dialysis*) and is made possible by the development of new, fully programmable, cyclers pumps. Since DPD enjoys a larger number of degrees of freedom in specifying the pattern of  $\varphi$  with respect to more classical CCPD or APD, its prescription has to be provided directly by a numerical optimization process. To this aim we need to set up a *multi-objective optimization strategy* that allows us to take into account the several factors coming into play with different weights. This requires to identify a global efficiency parameter  $\eta$  whose maximum within the therapy constraints would provide the optimal therapy.

Let  $\eta = \eta(\varphi)$  describe the relationship between the efficiency and the input profile. Then a control problem can be formulated as follows

$$\text{find } \varphi \text{ such that } \eta(\varphi_{opt}) = \max_{\varphi} \eta(\varphi)$$

To solve this problem the optimization algorithm used is based on the Pontryagin's Maximum Principle (see [Wei]), and it consists of an iterative process that starts at an initial guess  $\varphi_0$ , corresponding to a standard therapy, for instance an APD. By solving the PD problem and a related problem the *adjoint problem*, it is possible to find a sequence of iterates  $\varphi_n$  ( $n = 1, 2, \dots$ )

that converges to the optimal one. The numerical algorithm terminates when the optimum has been approximated with sufficient accuracy. The algorithm requires to run a numerical simulation of the PD problem for different values of  $\varphi$  at each iteration. For instance, by assuming  $w_1 = 1, w_2 = w_3 = 0$  (that means that we optimize the  $KT/V_{urea}$ ) starting with a standard therapy profile (Fig. 22 left),  $KT/V_{urea}$  is improved as indicated in Tab. 1. The associated “optimal” profile is depicted in Fig. 22 right. Since the optimization procedure is rather efficient it may be directly coded in the software that drives the cycler.

Iterations	$KT/V_{urea}$	% improvement
0	1.3299	0
10	1.3354	0.4
30	1.3554	1.9

**Table 1.** Improvement in  $KT/V_{urea}$  yielded by the optimization algorithm

This new simulation environment is opening new perspectives for a PD treatment carried out at patients’ home. By means of mathematical tools, the therapy is actually tuned in the “best” way for the individual patient who may chose the shortest therapy for a given efficiency target, or the more efficient therapy for a given period of dialysis. Furthermore, sensors measuring the concentrations in the patient may provide a feedback control. The mathematical model can then be improved by a “data assimilation” procedure, that adapts the therapy constantly.

## 2.6 Anastomosis shape optimization

### *The problem*

When a coronary artery is (partially or totally) occluded, blood is unable to oxygenate the heart muscle properly. The oxygen supply can be restored surgically by means of a bypass from aorta to the coronary artery downstream the occlusion. Various implant procedures and bypass types are currently available (see Fig. 24). A bypass can be made up either by organic material (e.g. the saphena vein taken from one of the patients legs, or the mammary artery) or by prosthetic material. They may feature very different shapes, such as, e.g., cuffed arteriovenous access grafts.

Current statistics [HCOL05] show that unfortunately 18% of patients who undergo surgery for a bypass implant risk re-occlusion and the 80% of bypasses implanted must be replaced after 10 years. The repetition of surgical procedures involves a high risk of complications. This is why it is worthwhile to investigate the aspects that may cause complications and post-operative

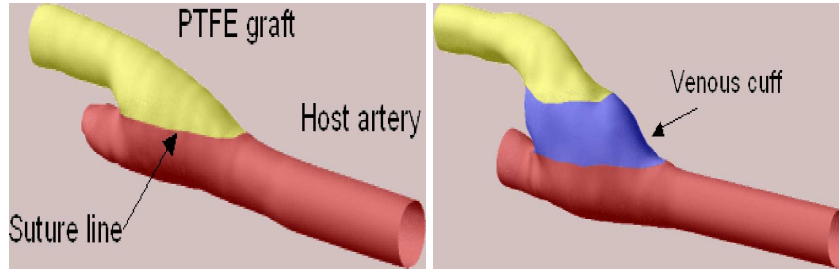


**Fig. 24.** Two different possible morphological variants of a coronary by-pass (from the web site [www.numerik.math.tugraz.at/biomech/cfd/selected\\_studies/flow.html](http://www.numerik.math.tugraz.at/biomech/cfd/selected_studies/flow.html), courtesy of K. Perktold, M. Prosi.). On the left a conventional procedure, on the right the so-called Miller Cuff.

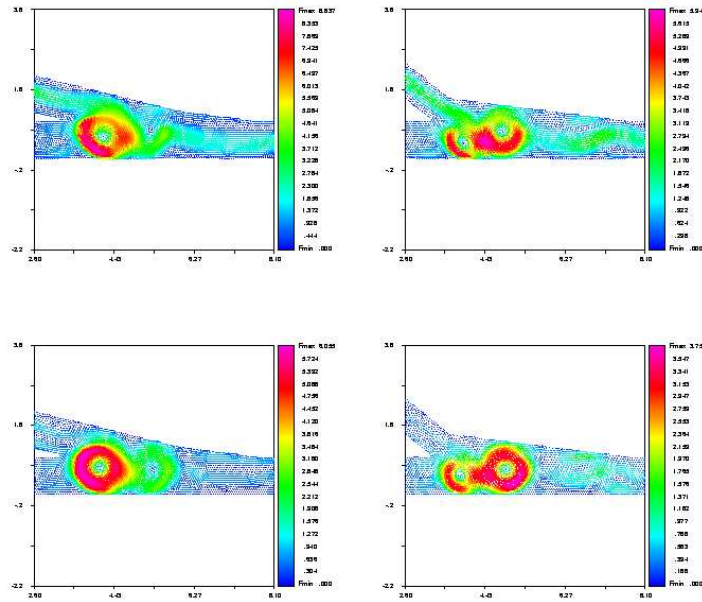


**Fig. 25.** Velocity field during diastole in two different models of a by-pass

failures, such as recirculation, abnormal disturbed flows, re-stenoses, hyperplasia etc., with the aim of finding the strategy for their reduction.

In Fig. 25 we illustrate some simulations in two simplified anastomoses, highlighting the impact of the angle between the stenosed branch and the graft on the downstream haemodynamics during the diastole. As a matter of fact, mathematical shape optimization tools can be applied for suggesting optimized configurations at various levels, from the local geometry (especially in implant area), to the quantities that form the entire bypass structure (im-

plant angle, ratio between bypass diameter and the artery in the implant area, distance between the new implant and the stenoses etc.).

Shape optimization is currently applied in many engineering fields (see e.g. [Pir84]) and, in principle, can be extended to many biomedical applications. Here, the domain of interest is not given, as it is the outcome of the computation. The goal is to find the domain that allow to fulfill some requirements for the velocity and pressure fields, which are normally specified as the minimum of suitable cost functional, subject to constraints. This procedure implies high computational costs that have prevented so far its practical application in surgical planning. Here we present however some basic results.

We mention that besides the problem we are considering here, shape optimization techniques could be applied as well to the FloWatch device discussed in a previous Section.

This research is carried out in cooperation with A. Patera (MIT, Boston) and V. Goshkhov (Russian Academy of Sciences, Moscow).

### *Numerical models and simulations*

*Approaches of Control and Shape Design.* Our goal is to find a geometrical configuration of the anastomosis which could reduce the downstream (or distal) occlusion risk, which in tuurn is related to the local haemodynamics generated by the bypass. To this aim, we need to (i) find an appropriate cost function, related to the local haemodynamics and which measures how the latter affects the distal re-stenosis risk and (ii) devise a procedure to find the bypass shape that reduce, among alla admissible shapes, the risk.

Some physical quantities, often called *indexes*, have been proposed in order to measure the re-occlusion risk (the Oscillatory Shear Index, the Mean Wall Shear Stress Gradient, the Oscillatory Flow Index). They are all derivated from the velocity and pressure fields that can be computed by solving the Navier-Stokes equations (1) around the anastomosis region. In the optimization process, these equations play the role of *state equations*, establishing the relations between the control variables (the shape of the domain) and the function to be controlled. As a cost functional, here we have chosen a measure of the *fluid vorticity* in the domain since it has been found that all the previous indexes have a favorable value in a flow with low vorticity. So it seems resonable to take it as a possible indicator for an anomalous downstream conditions induced by the anastomosis (see Fig. 25). More precisely, if  $\Omega_d$  denotes the anastomosis downstream region, a reliable cost functional is (see [QR03]):

$$\mathcal{J}(\mathbf{u}) \equiv \int_{\Omega_{wd}} |\nabla \times \mathbf{u}|^2 d\mathbf{x}. \quad (22)$$

The second issue can be faced with (at least) two different approaches. In the first one, the domain is locally deformed by moving each point on the boundary following the indication of the optimization algorithm. In practice, this means that the Navier-Stokes equations are discretized (e.g. by Finite

Elements) on a computational mesh, then the optimization algorithm will compute the displacement of the boundary nodes. The mesh will be deformed or recomputed correspondingly (see Fig. 26, left top).

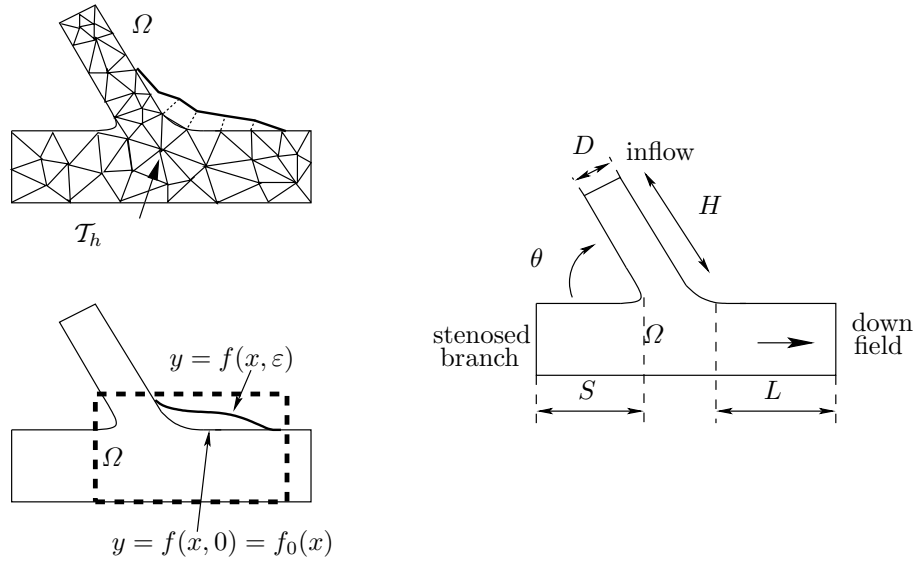


**Fig. 26.** Shape control approaches: local optimization based on the local control of the nodes (left, top), local control based on perturbation theory (left, bottom), global control based on a few geometrical parameters (right)

A different approach is based on the perturbation theory. Suppose that the boundary to be adjusted could be described by the function  $f(x, \varepsilon)$  (see Fig. 26, left bottom), and in particular that the dependence on the parameter  $\varepsilon$  could be expressed as

$$f(x, \varepsilon) = f_0(x) + \varepsilon f_1(x) + \varepsilon^2 f_2(x) + \dots,$$

where  $f_0(x)$  corresponds to the unperturbed shape. The Navier-Stokes solutions  $\mathbf{u}$  and  $p$  are assumed to be regular functions of the parameter  $\varepsilon$ , so that the expansions  $\mathbf{u} = \mathbf{u}_0 + \varepsilon \mathbf{u}_1 + \varepsilon^2 \mathbf{u}_2 + \dots$  and  $p = p_0 + \varepsilon p_1 + \varepsilon^2 p_2 + \dots$  make sense. The optimal control theory can be used for computing  $f_i$  by solving the problem for the first perturbations  $\mathbf{u}_i, p_i, i = 1, 2, \dots$

In the sequel, we will briefly address the first approach. The reader interested to the second one is referred to [AQR05].

We point out that it is possible to achieve the optimization also at a different, more global, geometrical level, by considering the configuration of the whole by-pass parametrized with a few geometrical quantities (see Fig. 26, right), for instance the length and the angle of the graft, the distance between the anastomosis and the stenosis, etc. The two optimization levels

(local and global) can be suitably combined. Actually, the global optimization can be faced with the so-called *Reduced Basis Techniques*, which can obtain “optimal” parameter estimates with a low computational cost. The results of this step can be used as the initial configuration of the local shape optimization (see [Roz04]).

*Results* The mathematical basic ingredients for an optimal control problem are:

1. a *control variable* (possibly a vector of scalar variables), belonging to a functional space  $\mathcal{U}$  of admissible controls;
2. the *state equations*, that represent the physical system to be optimized. For the sake of simplicity, in the numerical simulations presented hereafter we refer to the steady linear Stokes problem;
3. the *cost functional*  $\mathcal{J}$ : in our case, we choose (22).

The general statement of the problem then reads

$$\text{find } w \in \mathcal{U} \text{ such that } \mathcal{J}(w) \leq \mathcal{J}(v), \quad \forall v \in \mathcal{U}.$$

The minimization can be obtained iteratively. Starting from a given configuration, the state problem, suitably discretized, is solved to estimate the cost functional. The boundary deformation is suggested by a descent gradient-type method (see [Pir84]). This step requires the evaluation of the cost functional gradient  $\mathcal{J}'$  which is computed by solving another partial differential system, the *adjoint problem*. When the displacement is computed, the domain is moved and the mesh is deformed accordingly. The loop continues until a given stopping criterion is satisfied.

Figure 27 illustrates the results obtained by this algorithm: at the top-left the initial unperturbed configuration while in clockwise order we have configurations featuring 22%, 38% and 45% (optimal shape) vorticity reduction. The full loop has been carried out in 25 iterations. It is interesting to highlight that the optimal shape resembles a kind of intervention in use in the surgical practice, called Taylor patch (see [QR03]). Therefore, control theory furnishes in this case a possible rigorous “explanation” to a practice so far based only on intuitions and experience.

### 3 A wider perspective

In this work we have presented just a few practical examples where the mathematical and numerical modeling of the cardiovascular system has given relevant contributions, and probably will give even more important ones in the future. Many other problems with a relevant medical interest have been investigated by developing mathematical models and numerical methods. We quote, for instance, the vessel tissue dynamics and the mechanics of the heart

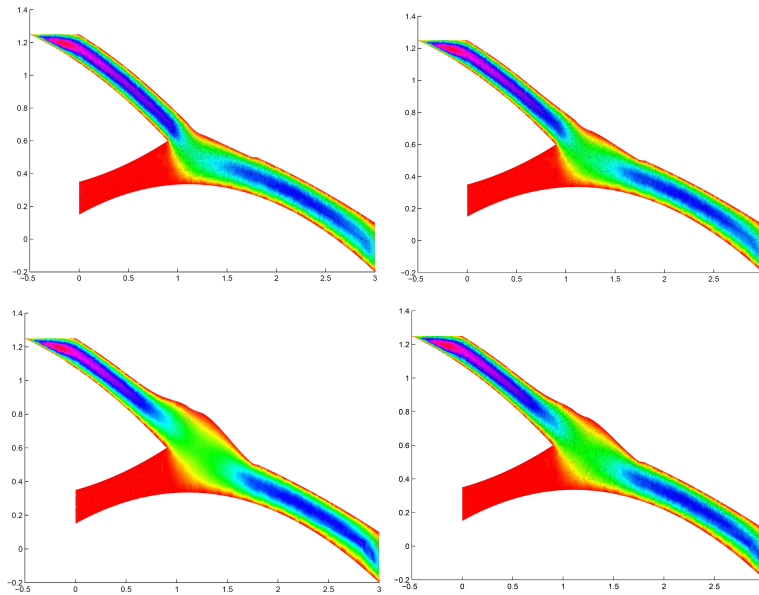


**Fig. 27.** Different solutions found during the shape optimization process: initial shape is at the top-left and in clockwise order we have shapes featuring 22%, 38% and 45% reduction in vorticity (courtesy of G. Rozza)

wall. These problems stimulate the development of accurate and computationally affordable models for biological tissues. The description of the mechanics of the walls is quite often based on the definition of a *strain energy density function*, whose derivatives yield the components of the stress-deformation tensor. An overview of recent contributions in this field can be found in [Tel05]. In particular, concerning the heart mechanics and functionality, recent investigations show that the ventricular myocardium can be unwrapped by blunt dissection into a *single continuous muscle band* (see [TG73]): this anatomical evidence could be included in mathematical models for the heart mechanics. Correspondingly, numerical methods for the simulation of the fluid-structure interaction in arteries and in the heart have been extensively investigated. The *immersed boundary method* proposed by C. Peskin for the heart dynamics in 1970's is receiving growing attention in different fields of computational biology (see e.g. [PM89, MI05]). Other methods based on the iterative solutions of fluid and structure problems and the *Arbitrary Lagrangian Eulerian* approach for managing the mesh motion have been investigated in the last years (see [GVF05], [DF03], [DDFQ05]). Following this approach, the fluid-structure interaction problem is split at each time level into the separate computation of the fluid velocity and pressure fields and of the structure displacement, together with the computation of the stress on the wall (that typically is used as a boundary term for the structure solver) and the mesh displacement ALE

computation. This research has yielded a 10 times reduction in CPU time for a typical haemodynamic simulation, even if for stability reasons about  $10^4$  time steps are needed for one second of time simulated (about one heart beat). This stimulates active research for achieving more effective methods.

In Fig. 28 we report some snapshots (taken from [DDFQ05]) of a fluid-structure simulation in a carotid artery obtained with this method, implemented in the code LifeV (see [www.lifev.org](http://www.lifev.org)).

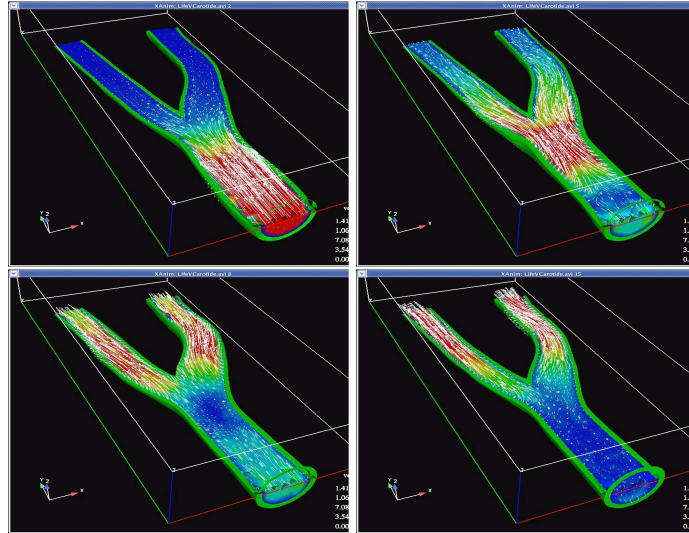


**Fig. 28.** Snapshots of a fluid-structure interaction simulation in a compliant carotid artery (courtesy of G. Fourestay)

Another issue that we have not considered in our overview is the *temperature* and its role in the physiology and also in some medical treatment, like the hyperthermia therapy in oncology [SGR<sup>+</sup>03].

In this context, and in general in the field the microcirculation, modelling requires mathematical techniques for the correct description of the behavior of heterogeneous media featuring small scales with respect to the scale of interest.

Besides the problems just mentioned, which belong to the *core* of computational haemodynamics, other relevant topics strictly related to the numerical computing are to be addressed, concerning the pre- and post-processing in blood flow simulations. The *accurate geometrical reconstruction* from medical images is an important and active field of research (see e.g. [Ste02]); in particular, the impact of geometrical modeling on the accuracy and reliability of numerical simulations is a crucial aspect still to be extensively investigated. On the other side, an *effective synthesis of the large amounts of data* obtained by numerical simulations is of paramount relevance for the medical purposes.

In fact, the definition and accurate computation of a few quantities or indexes, able to summarize the relevance of a pathology, like for instance the residence time inside an aneurysm is a decisive step in translating numerical results into practical indications for the medical doctors.

The cases study presented and these final comments witness the great development of mathematical and numerical models for the cardiovascular system in recent years. Some basic aspects of the problems at hand have been understood and in some cases this yielded some practical answers. The future challenges will concern the numerical *integration* of the basic components developed so far. Quoting [CHH<sup>+</sup>04], this goal can be regarded in the framework of the set up of: “*in silico* organs, organ systems and, ultimately, organisms. In silico models will be a crucial tools for biomedical research and development in the new millennium, extracting knowledge from the vast amount of increasingly detailed data, and integrating this into a comprehensive analytical description of biological functions with predictive power: the Physiome.” The present overview pinpoints the need of modeling complex, heterogeneous and interacting dynamics, ranging from the single cell dynamics up to complex network analysis. An instance of the most interesting tasks of such “in silico” vision, is the coupled electrical and mechanical simulation of the heart.

The complexity of the subject reflects also in the necessity of integrating different mathematical and numerical tools in the same solution environment. For instance, statistical and numerical tools could be integrated in establishing correlations among clinical data, understanding their driving mechanisms and defining precise decision trees, which are a quite common tools in clinical practice. The effective integration of mathematical/numerical methods can be therefore figured out as the key answer to the new (or even old) challenges of vascular medicine and surgery.

## Acknowledgements

Authors wish to thank all the persons involved in the various projects addressed in this work: in no specific order, we mention A. Corno (Liverpool), C. D’Angelo, D. Mastali, G. Rozza (CMCS-EPFL, Lausanne), F. Nobile, M. Prosi, P. Zunino (MOX, Politecnico di Milano Milan), S. Deparis (MIT, Boston), G. Dubini, F. Migliavacca, G. Pennati, R. Balossino, K. Laganà (LABS, Milan), M.A. Fernandez, J.F. Gerbeau (INRIA, Paris). This work has been made possible by the INDAM support through the Project: “Integrazione di Sistemi Complessi in Biomedicina: modelli, simulazioni, rappresentazioni” and the EU Project HPRN-CT-2002-00270 “HaeModel”.

## References

- [AQR05] Agoshkov V., Quarteroni A., and Rozza G. (2005) Shape design in aorto-coronary bypass using perturbation theory. to appear in SIAM J. Num. Anal.

- [ASON05] American-Society-Of-Nefrology (2005) [www.asn-online.org](http://www.asn-online.org).
- [Bov98] Bove E. (1998) Current status of staged reconstruction for hypoplastic left heart syndrome. *Pediatric Cardiology* 19: 308–315.
- [CFvSS02] Corno A., Fridez P., von Segesser L., and Stergiopulos N. (2002) A new implantable device for telemetric control of pulmonary blood flow. *Interactive Cardiovascular and Thoracic Surgery* 1: 46–49.
- [CHH<sup>+</sup>04] Crampin E., Halstead M., Hunter P., Nielsen P., Noble D., Smith N., and Tawhai M. (2004) Computational physiology and the physiome project. *Experim Physiol* 89: 1–26.
- [CK02] Canic S. and Kim E. (2002) Mathematical analysis of the quasilinear effects in a hyperbolic model of blood flow through compliant axisymmetric vessels. *Mathematical Methods in Applied Sciences* (to appear).
- [CPF<sup>+</sup>05] Corno A., Prosi M., Fridez P., Zunino P., Quarteroni A., and von Segesser L. (2005) No more pulmonary artery reconstruction after banding. submitted to The Journal of Thoracic and Cardiovascular Surgery.
- [CSB<sup>+</sup>03] Corno A., Sekarski N., Bernath M., Payot M., Tozzi P., and von Segesser L. (2003) Pulmonary artery banding: long-term telemetric adjustment. *European J. of Cardio-thoracic Surgery* 23: 317–322.
- [Cur84] Curry F. (1984) *Handbook of Physiology*, chapter 8: Mechanics and thermodynamics of transcapillary exchange. American Physiological Society, Bethesda, Maryland, 1984. E.M. Renkin ed.
- [D'A05] D'Angelo C. (2005) Mathematical modelling of the cardiovascular system and skeletal muscle interaction during exercise. In Cancès E. and Gerbeau J.-F. (eds) *ESAIM-Proceedings*, volume 14, pages 72–88.
- [DDFQ05] Deparis S., Discacciati M., Fourestey G., and Quarteroni A. (2005) Fluid-structure algorithms based on Steklov-Poincaré operators. to appear in *Comp Meth Appl Mech Eng*.
- [DF03] Deparis S., Fernandez M. A., and Formaggia L. (2003) Acceleration of a fixed point algorithm for fluid-structure interaction using transpiration conditions. *M2AN* 37(4): 601–616.
- [FGNQ02] Formaggia L., Gerbeau J. F., Nobile F., and Quarteroni A. (2002) Numerical treatment of defective boundary conditions for the Navier-Stokes equation. *SIAM J Num Anal* 40(1): 376–401.
- [FLQ03] Formaggia L., Lamponi D., and Quarteroni A. (2003) One dimensional models for blood flow in arteries. *Journal of Engineering Mathematics* 47: 251–276.
- [FNQV99] Formaggia L., Nobile F., Quarteroni A., and Veneziani A. (1999) Multi-scale modelling of the circulatory system: a preliminary analysis. *Computing and Visualisation in Science* 2: 75–83.
- [FQ04] Formaggia L. and Quarteroni A. (2004) *Computational Models for the Human Body*, N. Ayache (ed.), chapter Mathematical Modelling and Numerical Simulation of the Cardiovascular System. Handbook of Numerical Analysis. Elsevier Science, Amsterdam.
- [Fry87] Fry D. (1987) Mass transport, atherogenesis and risk. *Atherosclerosis* 7(1): 88–100.
- [FV03a] Formaggia L. and Veneziani A. (2003) *One dimensional models for blood flow in the human vascular system*. Von Karman Institute Lecture Notes, Seventh Lecture Series on Biological Fluid Dynamics.

- [FV03b] Formaggia L. and Veneziani A. (2003) *Reduced and Multiscale Models for the Human Cardiovascular System*. Von Karman Institute Lecture Notes, Seventh Lecture Series on Biological Fluid Dynamics.
- [FV05] Formaggia L. and Veneziani A. (2005) Geometrical multiscale models for the cardiovascular system. to appear in T. Kowalesky (ed.) *Blood Flow Problems 2005*, Warsaw.
- [GBPD<sup>+</sup>02] Gokal R., Blake P., Passlick-Deetjen J., Schaub T., Prichard S., and Butkart J. (2002) What is the evidence that peritoneal dialysis is underutilized as esrd therapy? *Seminars in Dialysis* 15: 149–161.
- [GN84] Gokal R. and Nolph K. (eds) (1984) *The textbook of Peritoneal Dialysis, Peritoneal physiology-transport of solutes*. Kluwer Academic Publisher.
- [GVF05] Gerbeau J., Vidrascu M., and Frey P. (2005) Fluid-structure interaction in blood flows on geometries based on medical imaging. *Computers and Structures* 83: 155–165.
- [HCOL05] Health-Centers-On-Line (2005) [www.heartcenteronline.com](http://www.heartcenteronline.com).
- [HP92] Hoppensteadt F. and Peskin C. (1992) *Mathematics in Life Sciences and Medicine*. Springer-Verlag New York.
- [HRT96] Heywood J., Rannacher R., and Turek S. (1996) Artificial Boundaries and Flux and Pressure Conditions for the Incompressible Navier-Stokes Equations. *International Journal for Numerical Methods in Fluids* 22: 325–352.
- [KK58] Kedem O. and Katchalsky. A. (1958) Thermodynamic analysis of the permeability of biological membranes to non-electrolytes. *Biochimica et Biophysica Acta* pages 229–246.
- [KS98] Keener J. and Sneyd J. (1998) *Mathematical Physiology*. Springer-Verlag New York.
- [Lam04] Lamponi D. (2004) *One dimensional and Multiscale Models for Blood Flow Circulation*. PhD thesis, EPFL.
- [LBM<sup>+</sup>05] Lagana K., Balossino R., Migliavacca F., Pennati G., Bove E., de Leval M., and Dubini G. (2005) Multiscale modeling of the cardiovascular system: application to the study of pulmonary and coronary perfusions in the univentricular circulation. *J. Biomech.* 38: 1129–1141.
- [LDM<sup>+</sup>02] Laganà K., Dubini G., Migliavacca F., Pietrabissa R., Pennati G., Veneziani A., and Quarteroni A. (2002) Multiscale modelling as a tool to prescribe realistic boundary conditions for the study of surgical procedures. *Biorheology* 39: 259–364.
- [MBP<sup>+</sup>05] Migliavacca F., Balossino R., Pennati G., Dubini G., Hsiab T., de Leval M. R., and Bove E. L. (2005) Multiscale modelling in bio fluid dynamics: Application to reconstructive paediatric cardiac surgery. to appear in *J. Biomech.*
- [MCDG05] Martin V., Clement F., Decoene A., and Gerbeau J. (2005) Parameter identification for a one-dimensional blood flow model. *ESAIM PROCEEDINGS* 14: 174–200.
- [Met03] Metcalfe R. (April 2003) Editorial: The promise of computational fluid dynamics as a tool for delineating therapeutic options in the treatment of aneurysms. *Am. J. Neurorad* pages 553–554.
- [MI05] Mittal R. and Iaccarino G. (2005) Immersed boundary methods. *Ann. Rev. Fluid Mech.* 37: 239–261.
- [MP79] Moncrief J. and Popovich R. (1979) Continuous ambulatory peritoneal dialysis. *Contrib. Nephrol.* 17.

- [NL87] Nerem R. and LeVesque M. J. (1987) Fluid Mechanics in Atherosclerosis. In R.Skalak and Chen S. (eds) *Handbook of Bioengineering*. McGraw-Hill.
- [NO90] Nichols W. and O'Rourke M. (1990) *Mc Donald's Blood Flow in Arteries*. Edward Arnold Ltd. - London. Third edition.
- [Nor91] Norwood W. (1991) Hypoplastic left heart syndrome. *Annals of Thoracic Surgery* 52: 688–695.
- [OLG04] Oreopoulos D., Lobbedez T., and Gupta S. (2004) Peritoneal dialysis: where is it now and where is it going? *Int. J. Art. Organs* 27: 88–94.
- [Pir84] Pironneau O. (1984) *Optimal Shape Design for Elliptic Systems*. Series in Computational Physics. Springer-Verlag.
- [PM89] Peskin C. and McQueen D. (1989) A Three-Dimensional Computational Method for Blood Flow in the Heart - I Immersed Elastic Fibers in a Viscous Incompressible Fluid. *J. of Comp. Phys.* 81(2): 372–405.
- [QR03] Quarteroni A. and Rozza G. (2003) Optimal control and shape optimization of aorto-coronary bypass anastomoses. *M3AS* 13(12): 1801–1823.
- [QSS02] Quarteroni A., Sacco R., and Saleri F. (2002) *Numerical Mathematics*. Springer-Verlag.
- [QV99] Quarteroni A. and Valli A. (1999) *Domain Decomposition Methods for Partial Differential Equations*. The Clarendon Press Oxford University Press, New York. Oxford Science Publications.
- [QV03] Quarteroni A. and Veneziani A. (2003) Analysis of a geometrical multiscale model based on the coupling of ODEs and PDEs for blood flow simulations. *SIAM Mult Models Sim* 1(2): 173–195.
- [QVZ02a] Quarteroni A., Veneziani A., and Zunino P. (2002) A domain decomposition method for advection-diffusion processes with application to blood solutes. *SIAM J Sci Comp* 23(6): 1959–1980.
- [QVZ02b] Quarteroni A., Veneziani A., and Zunino P. (2002) Mathematical and numerical modeling of solutes dynamics in blood flow and arterial wall. *SIAM J Num An* 39(5): 1488–1511.
- [Rak04] Raker B. (2004) Researchers announce advances in medical models and tools for space exploration. *Northwest Science and Technology*.
- [Rip92] Rippe. B. (1992) A three-pore model of peritoneal transport. *Perit. Dial. Int.*, 13: 35–38.
- [Roz04] Rozza G. (2004) On optimization, control and shape design for an arterial bypass. *International Journal Numerical Methods for Fluids* 47(10-11): 1411–1419.
- [RP96] Rappitsch G. and Perktold K. (1996) Pulsatile albumin transport in large arteries: a numerical simulation study. *ASME J. of Biomech. Eng.* 118: 511–519.
- [RS04] Robertson A. and Sequeira A. (2004) A director theory approach for modelling blood flow in the arterial system. *M3AS*.
- [SGR<sup>+</sup>03] Sreenivasa G., Gellermann J., Rau B., Nadobny J., Schlag P., Deuffhard P., Felix R., and Wust P. (2003) Clinical use of the hyperthermia treatment planning system hyperplan to predict effectiveness and toxicity. *Int. J. Oncology Biol. Phys.* 55(2): 407–419.
- [SIK<sup>+</sup>03] Sano S., Ishino K., Kawada M., Arai S., Kasahara S., Asai T., Masuda Z., Takeuchi M., and Ohtsuki S. (2003) Right ventricle-pulmonary

- artery shunt in first-stage palliation of hypoplastic left heart syndrome. *J. Thor. Cardio. Surg.* 126: 504–509.
- [Ste02] Steinman D. (2002) Image-based CFD modeling in realistic arterial geometries. *Annals Biomed. Eng.* 30(4): 483–497.
- [Tel05] Telega J. (2005) *Modelling in Biomechanics*, chapter Modelling of Soft Tissues Behaviour, by J.J. Telega and M. Stanczyk. Number 19 in Lecture Notes. AMAS, Institute of Fundamental Technology Research, Warsaw, Poland.
- [Tem86] Temam R. (1986) *Navier-Stokes Equations, Theory and Numerical Analysis*. North-Holland, Amsterdam, 3rd edition.
- [TG73] Torrent-Guasp F. (1973) *The Cardiac Muscle*. Juan March Foundation.
- [VLMF91] Vonesh E., Lysaght M., Moran J., and Farrell P. (1991) Kinetic modeling as a prescription aid in peritoneal dialysis. *Blood Purif.*, 9: 246–270.
- [Wei] Weisstein E. Pontryagin maximum principle. [mathworld.wolfram.com/](http://mathworld.wolfram.com/).
- [Whi86] White F. (1986) *Viscous Fluid Flow*. McGraw-Hill NY.
- [Wol] Wolfram: [www.mathematica.org](http://www.mathematica.org).
- [WP04] Wang J. and Parker K. (2004) Wave propagation in a model of the arterial circulation. *J Biomech* 37: 457–470.
- [ZMQ<sup>+</sup>05] Zunino P., Mastalli D., Quarteroni A., VanBiesen W., Vecten D., Pacitti A., Lameire N., Neftel F., and Wauters J. (2005) Development of a new mathematical approach to optimize peritoneal dialysis. in preparation.
- [Zun04] Zunino P. (2004) Multidimensional pharmacokinetic models applied to the design of drug eluting stents. *Cardiov Eng.* 4(2).